České vysoké učení technické v Praze
Fakulta strojní

Biomechanics of vertebral compressive fracture

Diploma thesis

Štěpánka Haiblíková

Prague, 2018

ZADÁNÍ DIPLOMOVÉ PRÁCE

I. OSOBNÍ A STUDIJNÍ ÚDAJE

Příjmení: **Haiblíková** Jméno: **Štěpánka** Osobní číslo: **408892**

Fakulta/ústav: **Fakulta strojní**

Zadávající katedra/ústav: **Ústav mechaniky, biomechaniky a mechatroniky**

Studijní program: **Strojní inženýrství**

Studijní obor: **Biomechanika a lékařské přístroje**

II. ÚDAJE K DIPLOMOVÉ PRÁCI

Název diplomové práce:

Biomechanika kompresivní fraktury obratle

Název diplomové práce anglicky:

Biomechanics of vertebral compressive fracture

Pokyny pro vypracování:

1. Případová studie pacienta - klinická data
2. Přehled metod využitelných k řešení problému
3. Vytvoření 3D modelu páteře
4. Odhad zatížení páteře na jednotlivých úrovních
5. Odhad pevnosti obratlů na jednotlivých úrovních
6. Zhodnocení výsledků

Seznam doporučené literatury:

1. Brinckmann, P., M. Biggemann, and D. Hilweg. ?Prediction of the compressive strength of human lumbar vertebrae.? Clinical Biomechanics 4 (January): iii-27.
2. Michael A. Adams, The Biomechanics of Back Pain, 3rd ed. (Edinburgh: Churchill Livingstone/Elsevier, c 2013), 115-19.
3. M. Christophy. ?A detailed open-source musculoskeletal model of the human lumbar spine.? Master?s thesis, University of California at Berkeley, 2010.

Jméno a pracoviště vedoucí(ho) diplomové práce:

prof. RNDr. Matej Daniel, Ph.D., odbor biomechaniky FS

Jméno a pracoviště druhé(ho) vedoucí(ho) nebo konzultanta(ky) diplomové práce:

Datum zadání diplomové práce: **19.04.2018** Termín odevzdání diplomové práce: **17.08.2018**

Platnost zadání diplomové práce: _____

prof. RNDr. Matej Daniel, Ph.D.	prof. Ing. Milan Růžička, CSc.	prof. Ing. Michael Valášek, DrSc.
podpis vedoucí(ho) práce	podpis vedoucí(ho) ústavu/katedry	podpis děkana(ky)

III. PŘEVZETÍ ZADÁNÍ

Diplomantka bere na vědomí, že je povinna vypracovat diplomovou práci samostatně, bez cizí pomoci, s výjimkou poskytnutých konzultací. Seznam použité literatury, jiných pramenů a jmen konzultantů je třeba uvést v diplomové práci.

10. 05. 2018
Datum převzetí zadání

Podpis studentky

Annotation

Název DP:	Biomechanika kompresní fraktury obratle
Autor:	Štěpánka Haiblíková
Akademický rok:	2017/2018
Studijní program:	Strojní inženýrství
Obor:	Biomechanika a lékařské přístroje
Ústav:	Ústav mechaniky, biomechaniky a mechatroniky
Vedoucí práce:	prof. RNDr. Matej Daniel, Ph.D.
Počet stran:	75
Počet obrázků:	39
Počet tabulek:	6
Klíčová slova:	biomechanika lidského obratle, epilepsie, klinický případ, zlomenina bez vnějšího traumatu, mezní síla obratle, extrémní zatížení páteře, CT vyšetření
Anotace:	Tato studie poskytuje výpočetní podklad na podporu hypotézy, která předpokládá, že kontrakce zádových svalů při epileptickém záchvatu bez vnějšího poranění může způsobit zlomeninu obratle. Na základě biomechanické analýzy daného případu epileptického pacienta bylo stanoveno riziko pro vznik těchto zlomenin. Bylo zjištěno, že odhadované síly svalů při záchvatu mohou převýšit zátěž, při které dochází k selhání obratle. Závěrem práce tedy je, že svalová kontrakce během epileptického záchvatu může zapříčinit zlomeninu obratle. Proto je navrženo zahrnout CT vystření páteře do standardních klinických postupů při ošetření pacienta po epileptickém záchvatu v každém případě, kdy si pacient stěžuje na bolest zad.
Title of DP:	Biomechanics of vertebral compressive fracture
Keywords:	biomechanics of the human vertebra, epilepsy, clinical case, seizure-induced fracture, vertebral failure load, high spinal loads, CT examination
Abstract:	The study provides a computational support for the hypothesis that contraction of back muscles during an epileptic seizure with no external trauma may result in vertebral fractures. Based on biomechanical case analysis of a patient after an epileptic seizure, the fracture risk was estimated. The results showed that estimated muscle forces during the seizure may exceed the vertebral failure load. We conclude that muscle contraction during non-traumatic epileptic seizures may induce vertebral body fracture. Based on the study results, we propose to modify the standard clinical practice guidelines for post-epilepsy treatment by adding a CT examination if the patient complains of back pain.

Affirmation

I, Štěpánka Haiblíková, declare that I have composed my Master's Thesis independently, have not used other references than stated and have not used any illegitimate support.

In Prague: June 10, 2018 Signature:

Acknowledgement

I would first like to express my sincere gratitude to prof. RNDr. Matej Daniel, Ph.D., for his passionate attitude during the whole time of development of this study. I appreciate all of his precious time that he provided me, the useful comments and advice about the direction of the work. This study was created under his conscientious and patient supervision.

It was prof. MUDr. Marcela Grünerová Lippertová, Ph.D., from Third Faculty of Medicine at Charles University who suggested to investigate a cause of the injury of one of her patients and provided CT scans of the fractured spine. During the cooperation, she was always willing to help and consult the problem. I thank her for that.

I would also like to thank my colleagues, Vojtěch Nedvěd and Veronika Řeháková especially, for many inspiring discussions, group studying, friendly competition and mutual help during our studies of master's degree.

My last thanks belong to my family. I am grateful to my mother and sister, Adéla Haibliková and Vendulka Haiblíková, for their endless support and encouragement.

Contents

List of figures **7**

List of tables **8**

List of symbols and abbreviations **9**

1 Clinical case and the problem statement **11**

2 Literature review **13**

2.1 Epilepsy and review of case reports 13

2.2 Treatment for vertebral compressive fractures 16

2.3 Spinal load estimation approaches 17

2.3.1 Experimental measurements 17

2.3.2 Musculoskeletal modelling 18

2.3.3 Biomechanics of skeletal muscle 22

2.3.4 Musculoskeletal model of the thoracolumbar spine 24

2.3.5 Joints and coordinates in OpenSim 25

2.3.6 Segmental angles of thoracolumbar spine in hyperextension 26

2.4 Methods of vertebral failure load prediction 28

2.4.1 Regression model 28

2.4.2 FEM model 33

2.4.3 Assessment of bone mineral density from CT scans 34

2.5 Summary of the literature review 35

3 Thesis objective **36**

4 Methods **37**
4.1 Vertebral compressive force estimation . . . 37
4.1.1 Computational model definition . . . 37
4.1.2 Parameters assessment . . . 38
4.1.3 Muscle selection . . . 42
4.1.4 Equilibrium equation formulation . . . 42
4.2 Vertebral failure load prediction . . . 44
4.2.1 Assessment of bone mineral density . . . 44
4.2.2 Measurement of vertebral mid-plane area . . . 46

5 Results **47**
5.1 Main results . . . 47
5.2 Minor results . . . 53

6 Discussion **57**
6.1 Compressive forces on vertebrae . . . 57
6.2 Vertebral failure load . . . 60

7 Conclusion **62**

Appendices **63**

A Global coordinates of the joints **64**

B Muscle groups **65**

C Angles of vertebral mid-planes **69**

D Muscles included in the analysis **70**

References **71**

List of Figures

1.1 Sagittal view of the patient's CT examination where the fracture of T5-T7 vertebrae can be observed. 11

2.1 Illustration of the body position during an epileptic seizure in its (a) tonic and (b) clonic phase. Addapted from McKean, Sylvia C. Principles and Practice of Hospital Medicine, 2012 [7]. 13

2.2 Images of similar seizure-induced vertebral fractures which has been previously reported. (a) CT scan of the lumbar spine showing a fracture of L2 adapted from clinical report by Moscote-Salazar et al., 2015, (b) CT scan revealing fractures of L2 and L4 adapted from the study made by Mehlhorn et al., 2007 and (c) postoperative radiograph (left) and MRI (right) showing resection of the T6 and T7 vertebrae adapted from clinical report by Takahashi et al., 2002 [11, 13, 14]. 15

2.3 Illustration of operative treatment of vertebral compressive fractures by (a) kyphoplasty and (b) vertebral fusion, adapted from Mayfield Brain & Spine [21, 22]. 16

2.4 Schematic diagram of the implantation system for intradiscal measurement, adapted from the study of Wilke et al., 1999 [29]. 17

2.5 Resultant force in L4-S1 intervertebral joint divided into compressive force and anterior shear force, adapted from Joint Structure and Function: A Comprehensive Analysis by Lavangie et al., 2005 [33]. 18

2.6 Simplified two-dimensional model of lifting task taken as an example for illustration of the single-equivalent force method, adapted from Basic Biomechanics by Hall, 2015 [24]. Global coordinate system is located in lumbosacral joint. 19

2.7 Inverse dynamic model scheme [32]. 20

2.8 Forward dynamic model scheme [32]. 21

2.9 The arrangement of actin and myosin myofilaments within a sarcomere, adapted from The structure of the contract filaments by R. Craig, 1994 [35]. 22

2.10 Hill's model of muscle, addapted from A Model of the Lower Limb for Analysis of Human Movement by Edith M. Arnold et al., 2010 [36]. 23

2.11 Musculoskeletal model of thoracolumbar spine made by Bruno, Bouxsein and Anderson, 2015 [37]. (a) Skeletal model, (b) complete model with muscles. 24

2.12 Depiction of the coordinate system used in OpenSim, adapted from A detailed open-source musculoskeletal model of the human lumbar spine by M. Christophy, 2010 [42]. 25

2.13 Adjustment of the muscle group attachment and PCSA. (a) The level at witch an equivalent PCSA and AP/ML moment arm are calculated (b) *in vivo* measurement from the CT scan, (c) calculation of an equivalent muscle group PCSA and AP/ML moment arm from model. Adapted from Development and Validation of a Musculoskeletal Model of the Fully Articulated Thoracolumbar Spine and Rib Cage by Bruno et al., 2015 [37]. 27

2.14 The experiment set-up of the study performed by Brinckmann et al., 1988 [48]. 28

2.15 Summary of reported segmental trends in compressive failure load of isolated vertebral bodies throughout the thoracic and lumbar regions until the year of 1995, adapted from the study made by Singer et al., 1995 [50]. 30

2.16 Sex and age-related vertebral failure load measured by Bouxsein et al., 2006 [47]. 31

2.17 The linear combination of BMD and CSA used to estimate vertebral failure load (*p<0.004; AN, anorexia nervosa; C, lean controls; OB obese) according to Bachmann et al., 2017 [46]. 32

2.18 Estimated L3 compressive failure load in men and women matched for age according to Bruno et al., 2014 [49]. 32

2.19 The distribution of axial elastic modulus in a voxel-based finite element model of a vertebral body used for vertebral strength estimation, adapted from the study made by Crawford et al., 2002 [51]. 33

4.1 Musculoskeletal model in the neutral position and in the full extension of the thoracolumbar spine. (a) Neutral position of the body, (b) total extension of the thoracolumbar spine. 39

4.2 Illustration of angles between two adjacent vertebrae in OpenSim modelling software. 40

4.3 Muscle groups selected to be compressing spine during an epileptic seizure. . 42

4.4 Measurement of mean values of HU of muscle tissue and fat used for phantom-less calibration. 45

4.5 Measurement of the vertebral cross-sectional area and orientation in the transverse plane performed in ImageJ. 46

5.1 Comparison of the maximal compressive force induced by the back muscles and body weight on each vertebra of the thoracic spine and estimated ultimate load of the given vertebra. Vertebral failure load was predicted according to Brinckmann et al., 1988, with the use of regression coefficients for thoracic vertebrae [48]). 47

5.2 The component of the total compressive force given by the weight of the body part located above the vertebra. 48

5.3 Muscles groups and their fascicles selected to be compressing the fifth thoracic vertebra (T5). 49
5.4 Sagittal view of the muscle forces and body weight contributing to the resultant compressive force applied to vertebra T5. 49
5.5 Vertebral cross-sectional area measured in the transverse plane. 50
5.6 Prediction of vertebral failure load based on three different regression models with the use of BMD measured from the patient's CT scans. 51
5.7 Vertebral strength estimated based on different regression coefficients and measured BMD. 52
5.8 Global orientation of individual vertebrae in total extension. 53
5.9 The resultant force induced by back muscles and body weight. 54
5.10 Vertebral mid-plane area established analytically from the area measured in the transverse plane. 55
5.11 Mineral density of trabecular bone of each thoracic vertebra measured from patient's CT scans specified in grams of K_2HPO_4/ml. 56

6.1 Activation of individual fascicles compressing the fifth thoracic vertebra necessary to develop force equivalent to the vertebral ultimate load. 58
6.2 Comparison of the modelled spine curvature (global vertebral angles) and the curvature of the patient's spine. 59

D.1 Depiction of the back muscles included in the analysis. (a) Latissimus dorsi, (b) erector spinae, (c) multifidus, (d) quadratus lumborum (e) trapezius (f) neck muscles 70

List of Tables

2.1 Values of global angles of thoracolumbar spine in total extension adopted from previous experiments [31, 43]. Joint description refers to the adjacent vertebrae of the articulation, excursion is angular deflection in the sagittal plane in degrees. Negative values denote to a clockwise direction. 26

2.2 Results of the regression analysis made by Brinckmann et al., 1988. 30

5.1 Values of motion angles which were prescribed in the motion file setting the model into the desired position. Negative values denote to a clockwise direction. 54

A.1 Vertical position of the vertebral joints, assigned to the vertebra located below the joint. 64

B.1 List of the muscles groups included in the analysis after muscle elimination. Each muscle is divided into individual fascicles represented by its isometric force. Values taken over from the musculoskeletal model made by Bruno et al. [37]. 65

C.1 Angles between the tranverse plane and the vertebral mid-plane measured from patient's CT scans. 69

List of symbols and abbreviations

Symbols

α	... vertebral motion angle [°]
β	... vertebral global angle [°]
a	... neural activation [-]
BMD	... bone mineral density [mg/ml]
CSA	... cross-sectional area [cm^2]
E_{ave}	... average elastic modulus [MPa]
F_{FE}	... vertebral compressive failure load estimated by FEM [N]
F_{iso}	... maximal isometric force of the muscle [kN]
F^M	... muscle force [N]
F_U	... vertebral compressive failure load [kN]
H	... height of the vertebra [mm]
HU	... Houndsfield units [-]
K_{FE}	... vertebral stiffness estimated by FEM [N/mm]
l	... length [m]
L	... vertebral level [-]
M	... moment [Nm]
MMS	... maximum muslce stress [N/cm^2]
p	... probability value [-]
PCSA	... physiologic cross-sectional area [cm^2]
r	... moment arm
r^2	... coefficient of determination [-]
R^C	... compressive reaction force [N]
R^S	... shear reaction force [N]
t	... time [s]
v	... velocity [m/s]
W	... weight [N]

Abbreviations

AP	... anteroposterior
CaHA	... calcium-hydroxylapatite
CT	... computed tomography
cos	... cosine
DXA	... dual-energy X-ray absorptiometry
EMG	... electromyography
FEM	... finite element method
FEM	... finite element method
IAR	... instantaneous axis of rotation
K_2HPO_4	... dipotassium phosphate
L1-L5	... first till fifth lumbar vertebra
ML	... mediolateral
MRI	... magnetic resonance imaging
QCT	... quantitative computed tomography
ROM	... range of motion
S1	... first vertebra of the sacrum
sin	... sine
T1-T12	... first till twelfth thoracic vertebra

Chapter 1

Clinical case and the problem statement

A patient came to a chiropractor complaining of lower back pain after undergoing an epileptic seizure. This patient was a man at the age of 45, in a good physical condition, with no sign of osteoporosis. As he did not suffer from any external trauma, the source of the pain was attributed to a simple musculoskeletal sprain treated with a complex rehabilitation. After two weeks, the pain did not relent and thus a plain radiographic examination was conducted. The X-ray examination revealed fractures of the fifth, sixth and seventh thoracic vertebra (Fig. 1.1). The initial treatment of the patient was a complete contradiction to his real injury. Lower back pain is usually treated with rehabilitation and spinal mobilization while fractures have to be fixed and movement should be eliminated. Inappropriate treatment or delay in diagnosis might increase pain and prolong disability. Furthermore, there is a potential to cause iatrogenic injury of the spinal cord.

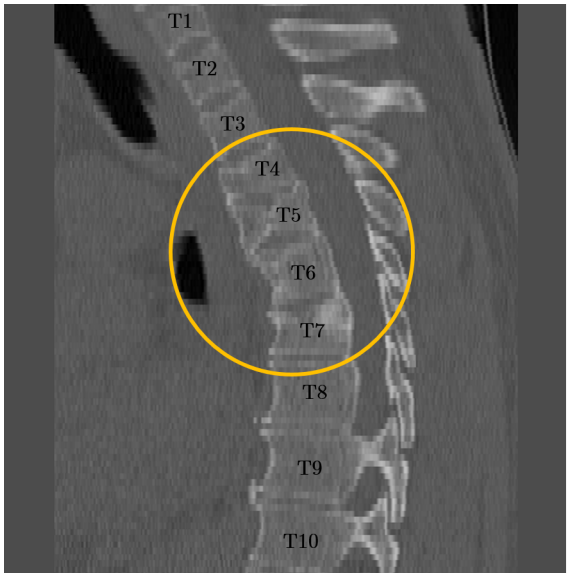

Figure 1.1: Sagittal view of the patient's CT examination where the fracture of T5-T7 vertebrae can be observed.

Misdiagnosis of the vertebral fracture is often a consequence of a doctors' unawareness of the risk of bone fractures resulting from extreme muscle stretch. Vertebral fractures have already been reported during electroconvulsive therapy in history. It is generally acknowledged that human vertebra fractures occur due to an injury where the force exerted against the bone is stronger than the bone can structurally withstand. A car accident, motorcycle crash, fall from height or sport related incident are some examples of such situations when extreme external forces are produced. Conversely, if the bone is weakened, the ultimate load which the vertebra is able to withstand is diminished and even normal daily activities can result in spinal fractures. People with vertebral fractures unrelated to trauma usually suffer from osteoporosis, tumours, spinal infections or other medical conditions. However, what might not be obvious is that someone can sustain a vertebral fracture even when that person suffers no external trauma and his bones are healthy.

The aim of this study is to provide an engineering insight into the mechanism of vertebral fractures during a tonic phase of an epileptic seizure by conducting a biomechanical analysis of a case on a given patient. The findings should provide a reliable support for the hypothesis that epileptic seizure-induced abnormal neural activity might produce a muscle stretch strong enough to result in vertebral fractures. The mission is to increase a doctors' awareness of muscle stretch being able to break a bone so that an early and appropriate treatment can be delivered to patients.

Chapter 2

Literature review

2.1 Epilepsy and review of case reports

In the literature, epilepsy is defined as a chronic disorder of the brain resulting in seizure episodes which happen due to excessive electrical discharges in a group of brain cells [1]. Seizures are caused by abnormal neuronal activity in the brain and if they occure repeatedly the condition is called epilepsy [2]. Epileptic seizures are characterized by involuntary movement that involves a part of the body (focal) or the entire body (generalized). Focal seizures start in a particular part of one side of the brain while generalized seizures affect both hemispheres and they are accompanied by loss of awareness [3, 4, 5]. Generalized epileptic seizure can cause muscle spasms, black out, or fall [4, 5, 6]. There are six types of generalized seizure, among which the most common one is a grand-mal, or tonic-clonic, seizure.

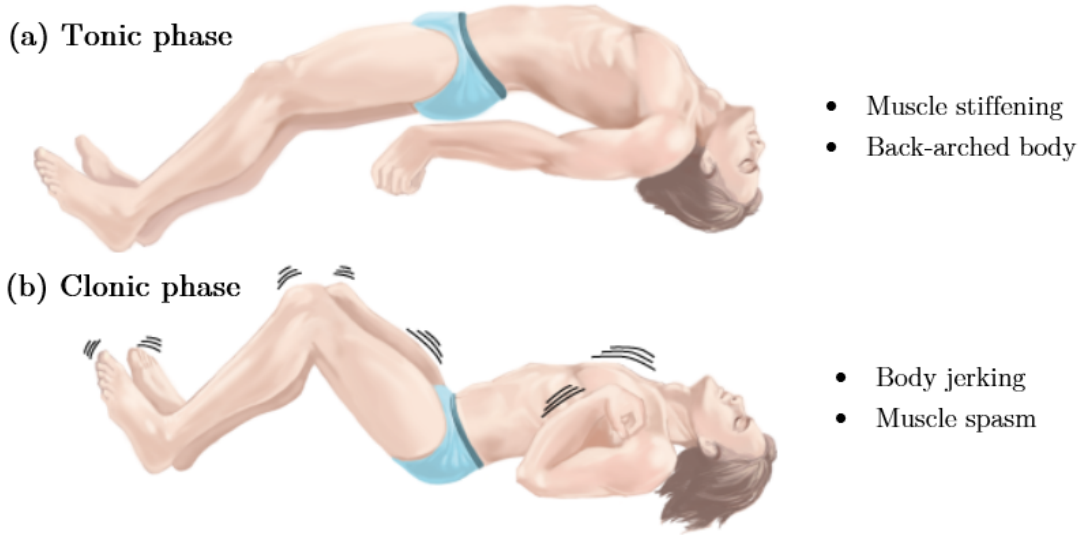

Figure 2.1: Illustration of the body position during an epileptic seizure in its (a) tonic and (b) clonic phase. Addapted from McKean, Sylvia C. Principles and Practice of Hospital Medicine, 2012 [7].

Tonic-clonic seizure has motor symptoms. As the name suggests, it has two stages. During a tonic phase of an epileptic seizure, lasting usually less than 20 seconds, muscles stretch and become rigid, the body is arched backwards and the patient stops breathing. Then the jerking movements happen in the clonic phase of the seizure. These episodes can result in physical injuries, including bone fractures which are usually attributed to an external trauma [5].

Although being rare, there are several cases reported where the vertebral fractures occured even in the absence of any external trauma. It was observed that most commonly these fractures occur in upper and middle thoracic spine. On the contrary, external trauma-induced fractures happen more often in lower thoracic and lumbar spine. The explanation for this phenomenon might be lower flexibility of the mid-thoracic spine and therefore higher vulnerability to the injury. Furthermore, higher concentration of the compressive forces during contraction of the muscles along the anterior and middle columns of the thoracic region might increase the risk of fracture as well [8, 9, 10].

Takahashi et al., 2002, reported a case similar to the one this study is investigating. A 34-year-old man complained of back pain after a generalised clonic convulsion lasting for a minute. Two weeks later, radiographs showed compressive fracture at T6 and T7 level. The bone mineral density of his vertebrae was reported to be decreased as a result of a treatment by antiepileptic drugs. It was observed that antiepileptic drugs increase fracture risk in epileptic patients by reducing BMD by up to 14%. It was noted that seizure-induced vertebral fractures happen mostly in adult males and that 40% of them occur unwitnessed in sleep. Particular emphasis was placed on the fact that vertebral fractures might be overlooked in patients with mild back pain [11].

In 2004, Gnanalingham et al. published a case report of a 26-year-old male who underwent a grand mal seizure while seated in a chair. Plain X-rays indicated compressive fracture at T5 and T6 level which was later confirmed by CT scans. The study suggested that CT or MRI examination should be performed rather than plain X-Rays as radiography fails to detect almost 25% of spinal fractures. It was also highlighted that seizure-induced vertebral fractures can be associated with back pain but they may as well be asymptomatic [12].

Another patient was reported to sustain vertebral fractures attributed to a violent muscle stretch during an epileptic seizure. Mehlhorn et al., 2007, described a case of a man at the age of 45 who suffered transverse fracture at L2 and burst fracture at L4 level. A cracking sound which woke up the patient from sleep indicated vertebral fracture and so the thorough examination was performed. Once more it was underlined that sizure-induced fractures can appear clinically asymptomatic and can easily be overseen due to absence of trauma [13].

Study made by Salazar et al., 2015, presented a case of an epileptic patient, 46-year-old male, who did not fall or undergo any external trauma and yet CT examination revealed fracture of the second lumbar vertebra. It was notified that violent forces generated during tonic-clonic seizure can cause axial skeletal trauma including thoracic and lumbar fractures. The fracture machanism was assumed to be the spinal hyperextension. It was also observed that clinical signs of unstable fractures can be subtle and so the study urged to radiologically examine the source of any back pain after seizures [14].

In 2016, 28-year-old man was presented to a chiropractor after a ten-day back pain at the mid-thoracic level initiated by a tonic-clonit seizure event. During the seizure, the patient was seated in a chair prevented from falling. Plain radiographic examination was conducted revealing compression fractures of T4 to T8. Stilwell et al., 2016, in this case report highlighted that delay in diagnosis or delivery of inappropriate treatment may be detrimental to the patient [15].

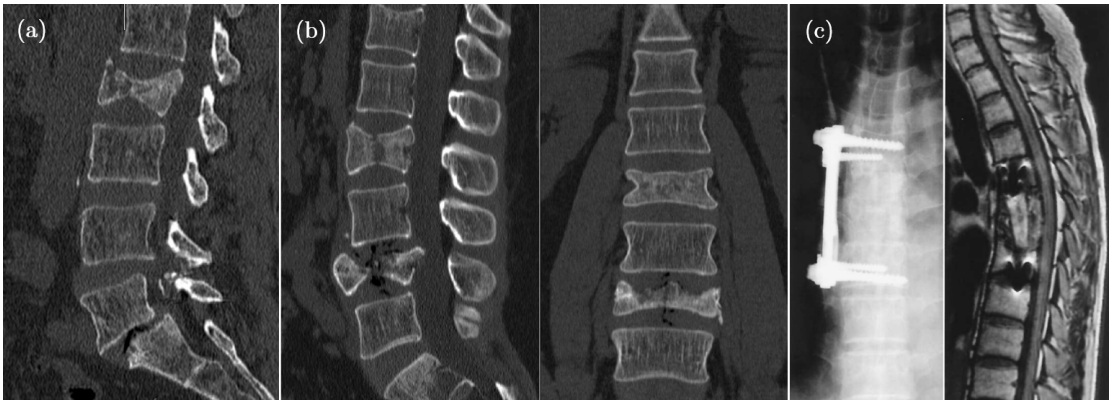

Figure 2.2: Images of similar seizure-induced vertebral fractures which has been previously reported. (a) CT scan of the lumbar spine showing a fracture of L2 adapted from clinical report by Moscote-Salazar et al., 2015, (b) CT scan revealing fractures of L2 and L4 adapted from the study made by Mehlhorn et al., 2007 and (c) postoperative radiograph (left) and MRI (right) showing resection of the T6 and T7 vertebrae adapted from clinical report by Takahashi et al., 2002 [11, 13, 14].

Overall, the vertebral fractures induced during a generalized epileptic seizure with no external trauma was reported for males at the age between 26-46 years. Most of the seizures were unwitnessed and occured during sleep. The emphasis was put on the fact that the symptoms may be mild and resemble simple acute mechanical back pain and so the vertebral fractures may be overlooked. Subtle spinal fractures may then be mistaken for a simple musculoskeletal sprain. Moreover, plain X-Rays of the spine might fail to detect approximately 22% of fractures. On this account, CT or MRI was suggested to be used for diagnosis [16, 17].

In the summary, it is reported that the vertebral fractures in the absence of external trauma were often misdiagnosed and not appropriately treated. It seems that it is not generally acknowledged that the fractures can happen as a result of the muscle stretch itself, however, the fractures caused by muscle forces have already been noticed in history during electro-convulsion therapy [8, 10]. It is believed that the violent forces generated by the strong paraspinal muscles during generalised tonic-clonic seizures are associated with vertebral fractures [6, 14]. Vertebral fractures following epileptic seizures are typically compression fractures, occurring in the mid thoracic region, although there are some cases reported in the lumbar region as well [8].

2.2 Treatment for vertebral compressive fractures

Nonoperative treatment for vertebral compression fractures includes pain medication and reduction in activity. Furthermore, back bracing might be used to limit the motion of fractured vertebrae by providing an external support to the injured spine. When chronic pain from a spinal compression fracture persists, surgical intervention is performed [18].

Vertebral compressive fractures are treated surgically by minimally-invasive techniques such as kyphoplasty or vertebroplasty. Both of these methods involve the percutaneous injection of bone cement directly into the fractured vertebral body [12]. In addition, kyphoplasty uses a balloon which forms a cavity inside the vertebral body as it inflates allowing for lower pressure of injection (Fig. 2.3). Reported results for both vertebroplasty and kyphoplasty show rapid improvement in pain and physical functioning in patients [19]. Additional potential of kyphoplasty is restoring vertebral height and reducing spinal kyphosis [20].

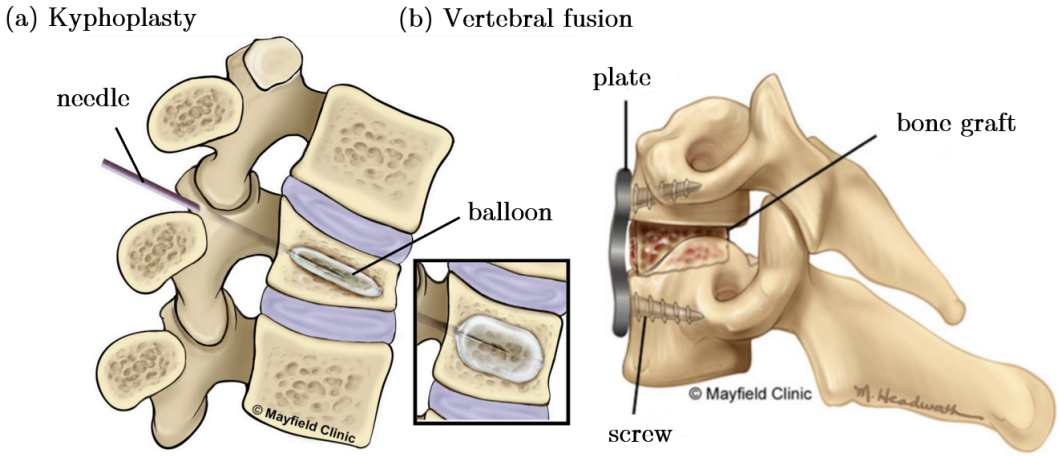

Figure 2.3: Illustration of operative treatment of vertebral compressive fractures by (a) kyphoplasty and (b) vertebral fusion, adapted from Mayfield Brain & Spine [21, 22].

Alternatively, vertebral compressive fractures can be treated with posterior fusion which eliminates motion between two vertebrae (Fig. 2.3) [14]. Posterior fusion is a process when a bone graft is used to cause the two adjacent vertebrae to grow together [23]. Another way of fracture stabilization present dorsally instrumented internal fixators. These include rods, hooks, plates, screws, or interbody cages aiming to provide internal support to the injured vertebra [13].

Regardless the method of fracture stabilization, the aim is to minimize the movement during the healing process while relieving the pain. That is a complete contradiction to the treatment of muscle strain for which the spinal fracture is often mistaken. Back pain originated from pulled back muscles or muscle strain is usually treated with a complex rehabilitation and spinal mobilization. Misdiagnosis and consequently inappropriate treatment of the vertebral fractures can prolong disability or even cause iatrogenic injury [15].

2.3 Spinal load estimation approaches

Analysis of spinal loads generally presents a complex and indeterminate mechanical problem. Body weight, external elements and muscles compensating for these external forces are not the only forces applied to the spine. Tension of the spinal ligaments, surrounding tissue and intraabdominal pressure contribute to the spinal loads as well. As the spinal muscles have extremely small moment arms, they must generate large forces to compensate the moments produced by the body weight and external loads. Consequently, the major force acting on the spine is usually the force induced by spinal muscles [24].

There are many approaches to assessment of the subject-specific spinal loading. Overall, these include either *in vivo* experimental measurement or neuromusculoskeletal modelling techniques. Using mathematical models to estimate the spinal loads, a limited number of activities can be analysed as the motion kinematics has to be well known. However, this technique became popular as it allows for an accurate theoretical motion analysis of the specific subject without any need of intervening with the patients's body [25, 26]. Experimental studies, on the other hand, although providing an accurate measurement, they might require relatively invasive procedure including implantation of instrumented devices or placing the needles into the subject's body [27, 28, 29].

2.3.1 Experimental measurements

In vivo measurement of the spinal compressive loads can be performed indirectly by means of the measurement of the intradiscal pressure and the cross-sectional area of the disc (Fig. 2.4). Questions might rise concerning the actual force compressing the vertebra as it is subjected to the mechanical properties of the disc and the level of its degeneration. Moreover, due to the heterogeneous material composition and the nonuniform load transfer within the disc, the calculation of compressive force by simple multiplication of the interdiscal pressure with the disc cross-sectional area seems to be inadequate. By employing a finite element model, the subject dependent correction coefficient was thus established to make the results more accurate [27, 29]. As low back pain affect the lower part of the lumbar spine, the previous studies focused on intradiscal pressure in L4-L5 intervertebral disc. Axial forces compressing the fift lumbar vertebra during spinal extension according to study made by Dreischarf et al., 2013, was established to be approximately 0.7 kN [30].

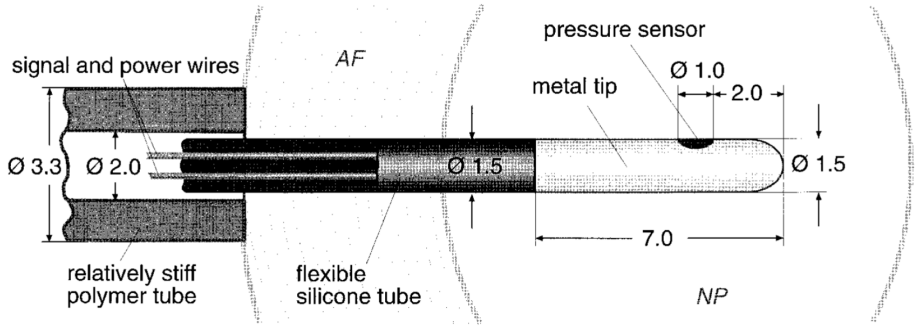

Figure 2.4: Schematic diagram of the implantation system for intradiscal measurement, adapted from the study of Wilke et al., 1999 [29].

Another way how to measure the compressive spinal loads *in vivo* is by means of instrumented implants. An instrumented vertebral body replacement allows measurement of the six force and moment components during activities of daily living. The forces applied to the implanted vertebral body replacement during the daily life activities were reported to reach up to 1.7 kN [28].

2.3.2 Musculoskeletal modelling

Musculoskeletal model is a widely used tool for determination of the forces on muscles, bones, and joints that are generally not measurable *in vivo*. Both static and dynamic models use basic principles of mechanics to estimate muscle forces and spinal loads subjected to different loading conditions. Musculoskeletal models employ free body diagram to maintain equilibrium equations between the known external loads and unknown internal forces. The equilibrium equations are usually composed in an imaginary plane cutted through the given intervertebral disc while computing the spinal loading. However, these equilibrium equations cannot be solved deterministically as the number of unknown inner forces considerably exceeds the number of available equations. For the analysis of the spinal loads, three approaches are commonly used: single-equivalent muscle, optimization-based, and EMG-assisted approach [24].

Single-equivalent muscle force method is based on replacing all of the muscle forces acting on a given part by a single resultant force. Once establishing the equivalent muscle force, joint reaction force can be calculated by satisfying force equilibrium equations. The resultant force applied to the given vertebra acting opposite to the calculated reaction force can be divided into its two components as shown in the Fig. 2.5. The component perpendicular to the mid-plane of the disc refers to the compressive force, and the other component parallel to the disc to the shear force. Furthermore, there is a lateral shear force in the direction perpendicular to the sagittal view which is usually considered negligible [31].

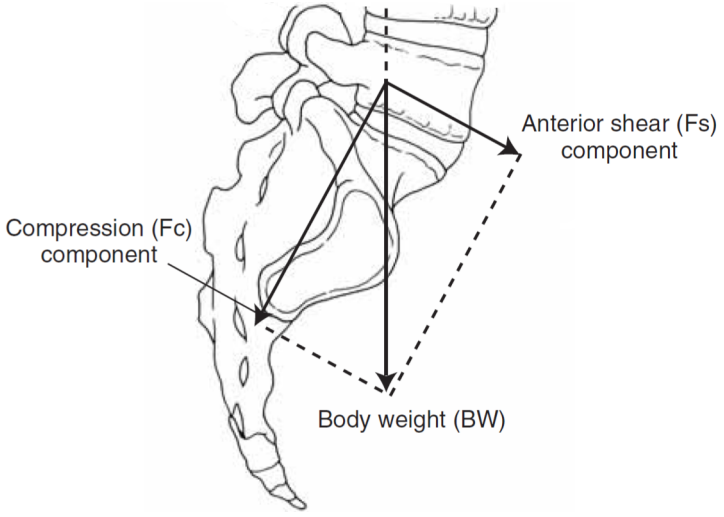

Figure 2.5: Resultant force in L4-S1 intervertebral joint divided into compressive force and anterior shear force, adapted from Joint Structure and Function: A Comprehensive Analysis by Lavangie et al., 2005 [33].

For illustration of the single-equivalent method, a static two-dimensional problem will be analysed (Fig. 2.6). The task of the given example is to determine reaction forces in the lumbosacral joint during a lifting activity (R^C, R^S). For those purposes, the force of back muscles and surrounding soft tissue is replaces by a single force (F^M) working againts external forces which are generating a clockwise moment. The equivalent muscle force is determined from moment equilibrium equation (Eq. 2.1). Subsequently, the two components of reaction forces, shear reaction force R^S and compressive reaction force R^C, are calculated from force equilibrium equations in x and y direction (Eq. 2.2, 2.3)).

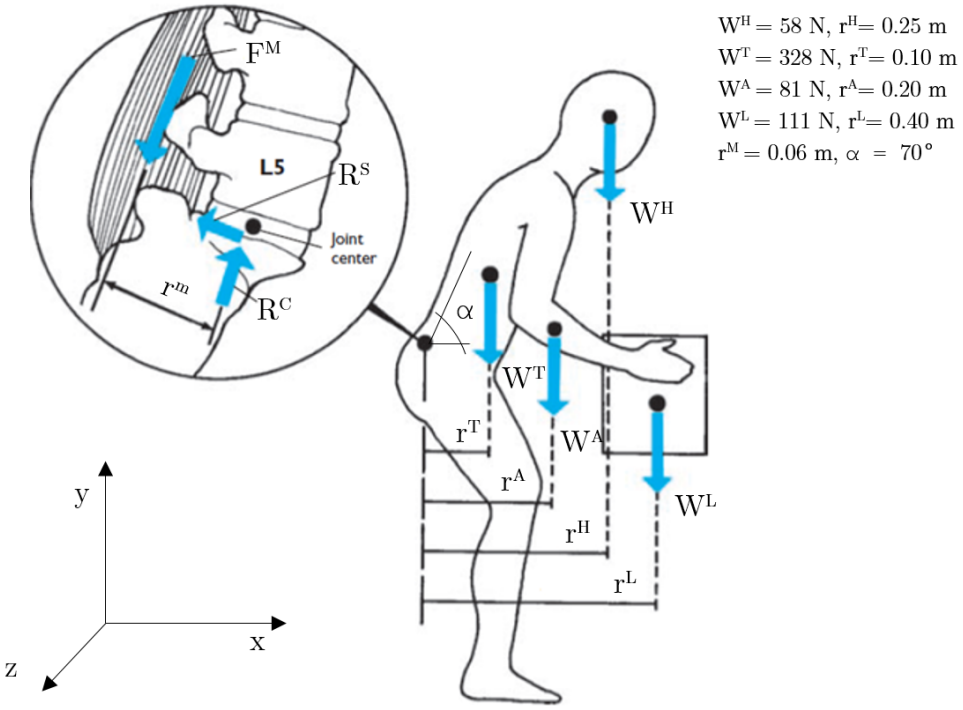

Figure 2.6: Simplified two-dimensional model of lifting task taken as an example for illustration of the single-equivalent force method, adapted from Basic Biomechanics by Hall, 2015 [24]. Global coordinate system is located in lumbosacral joint.

$$M_z : F^M \cdot r^m - W^H \cdot r^H - W^A \cdot r^A - W^T \cdot r^T - W^L \cdot r^L = 0 \tag{2.1}$$

$$F_x : R^C \cdot cos(\alpha) - R^S \cdot sin(\alpha) - F^M \cdot cos(\alpha) = 0 \tag{2.2}$$

$$F_y : R^C \cdot sin(\alpha) + R^S \cdot cos(\alpha) - F^M \cdot sin(\alpha) - W^H - W^T - W^A - W^L = 0 \tag{2.3}$$

where M_z in [Nm] is the moment along z axis, F^M in [N] is the muscle force, W^H, W^T, W^A, W^L in [N] are weights of head, trunk, arms and external load respectively, r in [m] is the moment arm of these forces in sagittal plane, R^C in [N] is the compressive reaction force and R^S in [N] is the shear reaction force, α in [°] is the angulation of the spine in lumbosacral joint.

Substituting the values, Eq. 2.1 is satisfied if single-equivalent muscle force F^M equals to 1.8 kN. From Eq. 2.2 and 2.3, calculated shear reaction force R^S and compressive reaction force R^C is 0.2 N and 2.3 kN respectively. The results show that the magnitude of shear reaction force is almost ten times lower that the magnitude of compressive reaction force.

So as to cope with the complexity of the problem while providing more precise estimation of the internal muscle forces, the musculoskeletal models have been developed. The principals of muculoskeletal modelling is well described in Routledge Handbook of Biomechanics and Human Movement Science written by Youlian Hong and Roger Bartlett, 2008 [32]. By means of neuromusculoskeletal modelling, as the name implies, the actions of muscle on the skeletal system are estimated as controlled by the nervous system. The muscle forces and thus the joint loading can be assessed by inverse or forward dynamics. As both of these techniques present certain limitations, forward-inverse or also called hybrid dynamics combining both of these approcahes has been introduced. The hybrid scheme estimates joint moments determined by both inverse and forward dynamics.

The musculoskeletal modelling is based on solving the motion equation for the particular joint given as:

$$M^J + m(q) \cdot \ddot{q} + C(q, \dot{q}) + G(q) + F_{ext} + M_{ext} = 0 \tag{2.4}$$

where M^J is the joint moment, m(q) presents segments' mass and inertial characteristics, external loading is given by external forces (F_{ext}) and moments (M_{ext})), G(g) is gravitational loading, $C(q, \dot{q})$ is centrifugal and coriolis loading and joint motion is given by its angle (q), angular velocity ($\dot{q}$) and angular acceleration ($\ddot{q}$).

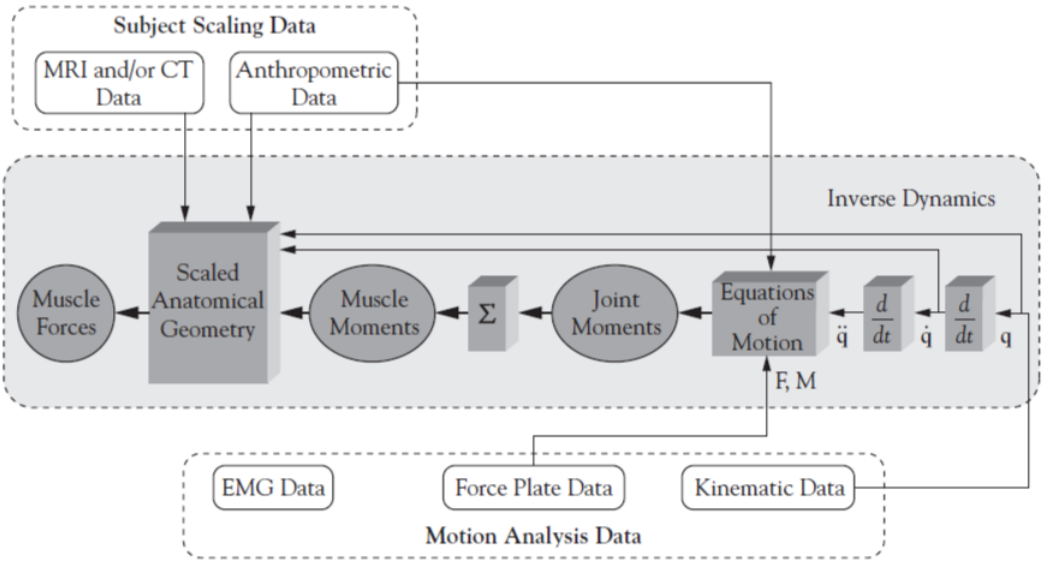

Figure 2.7: Inverse dynamic model scheme [32].

Using inverse dynamics (Fig. 2.7), the joint moment (M^J) is determined based on data collected in a motion analysis laboratory. The joint reaction forces are calculated as the sum of forces of muscle, ligament and surrounding soft tissue.

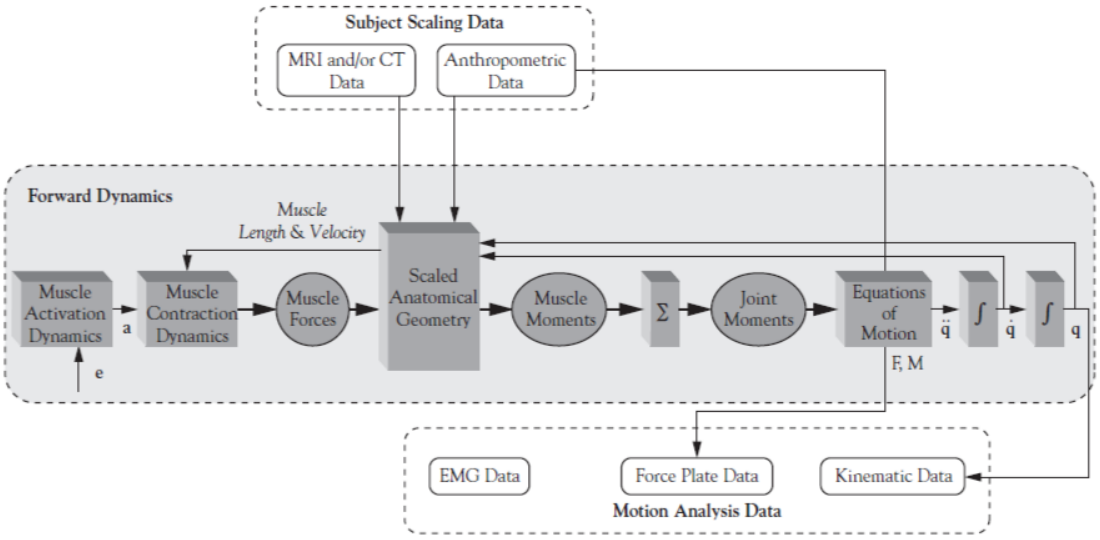

Figure 2.8: Forward dynamic model scheme [32].

In forward dynamics (Fig. 2.8), the equation of motion for the joint angular acceleration ($\ddot{q}$) is solved by specifying the joint moment which is given by the sum of individual muscle moments. The moment of individual muscles is calculated using the muscle moment arms and the force each muscle produce incorporating the action of each muscle driven by neural commands. Individual muscle forces are theoretically determined by means of a numerical optimization with an appropriately selected cost function minimizing muscle stress or summation of each muscle activation.

EMG-driven or EMG-assisted models use linear envelope of EMG signal to specify the neural command, instead of optimizing the muscle activations. In EMG-assisted models, the relationship between normalized EMG activity of the muscle and its force is presumed to estimate the individual muscle forces while satisfying the existing equilibrium equations. However, this approach is limited to superficial muscles and its accuracy is often questioned.

Musculoskeletal models usually include:

- The EMG-to-muscle/optimization-based activation dynamics model
- The model of musculoskeletal geometry
- Muscle contraction dynamics model
- Model calibration to a subject

Not only do the muscle forces depend on muscle activation but also the muscle kinematics has to be considered. Kinematics of the muscle are estimated using a model of the musculoskeletal geometry. Musculoskeletal softwares such as OpenSim (Simbios [34]) or AnyBody (AnyBody Technology, Denmark) are incorporating these musculoskeletal models using cadaveric data. These musculoskeletal models can be scaled to fit the subject-specific case either by anatomical markers placed on a subject during a motion capture session or by deforming and scaling an existing model.

2.3.3 Biomechanics of skeletal muscle

Muscle contraction dynamics model derives the muscle or musculotendon forces (F^{MT}) from muscle contraction dynamics and musculotendon kinematics. Most commonly, these models are based on a Hill-type theory of the muscle including the contractile element (muscle) in series with the passive element (tendon):

$$F^{MT}(t) = F_{iso}^{max}[f(l_M)f(v_M)a(t) + f_p(l_M)]cos(\psi(l_M)], \tag{2.5}$$

where $F^{MT}(t)$ is an instant force produced by the musculotendon unit, F_{iso}^{max} refers to the maximal isometric force of the muscle, $f(l_M)$ and $f(v_M)$ present the force dependance functions of the muscle force on its length and velocity respectively, $f_p(l_M)$ refers to the parallel passive elastic force-length curve, a(t) is the muscle activation and $\psi(l_M)$ pennation angle given by the muscle length.

For a better understanding of Eq. 2.5, biomechanics of muscle should be briefly presented. As the equation implies, muscle presents a complex biological structure with viscoelastic behaviour. Skeletal muscle is composed of muscle belly, comprising the muscle fibres, and the tendon that binds the muscle belly to the bone. A muscle fiber is a long cylindrical, multinucleated cell composed of smaller units of filament each containing a subunits called sarcomers. Each sarcomere comprises myofilamets, thin actin protein anchored at both ends of the sarcomere at the Z-line and thick myosin connected by titin. Sliding of the actin myofilament on the myosin chain is the basic mechanism of muscle contraction [24, 33].

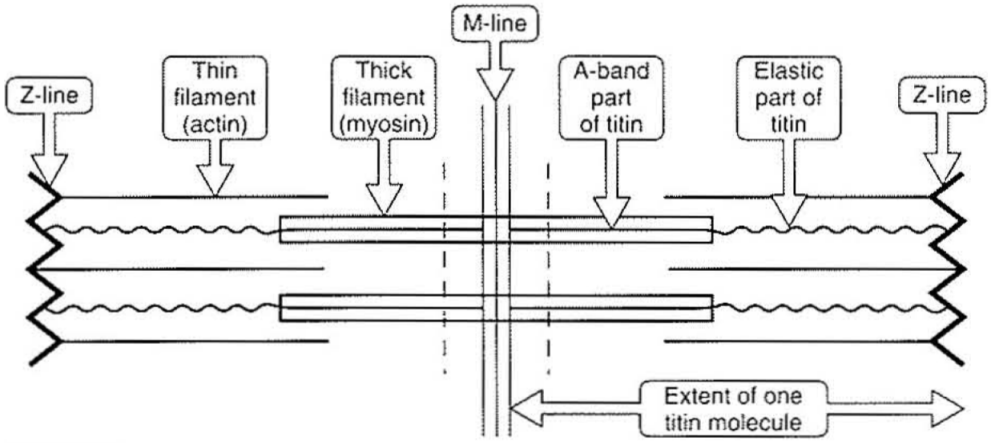

Figure 2.9: The arrangement of actin and myosin myofilaments within a sarcomere, adapted from The structure of the contract filaments by R. Craig, 1994 [35].

Muscles are the functional units of the musculoskeletal system that produce the motion at the joint. Their production of force and moment is the result of muscle contraction when the chemical energy is transformed to mechanical energy. Contraction is initiated by an electrical stimulus from neuron causing depolarization of the muscle fiber. When the fiber is depolarized, calcium is released into the cell and binds with troponin. The combination of calcium with troponin acts as a trigger, causing actin to bind with myosin, beginning the contraction [33].

Alterations in the proximity of the actin and myosin chains influence a muscle's force of contraction (active contractive element). The maximum number of cross-links between the actin and myosin myofilaments and hence the maximum contractile force in the sarcomere occurs when the full length of the actin chains is in contact with the myosin molecule, the state is refered as the resting length. However, the elastic properties of muscle's passive structure (epimysium, perimysium, endomysium and tendons) also influnce the force produced by the muscle. As the stretch of the muscle increases, the muscle exerts a larger pull against the stretch, caused by the elastic recoil of the passive structures (parallel passive element). The parallel element is responsible for the muscle passive behavior when it is stretched, even when the contractile element is not activated. The combined effects of muscle contraction and stretch of the elastic components are represented mechanically by a contractile element in series and in parallel with the series elastic components [24, 33].

Furthermore, eccentric, isometric and concentric contractions should be distinguished since the force produced by muscle is dependent on muscle's contractive velocity. Concentric contraction is defined as a contraction in which the muscle is shortened. Eccentric contraction occurs when there is a visible lenghtening of the muscle during. Isometric contraction has zero contraction velocity [33]. Hill derived a model of the muscle also known as three-element muscle model describing the muscle's mechanical response. The model is constituted by a contractile element in parallel with non-linear spring elements connected to another spring element (Fig. 2.10).

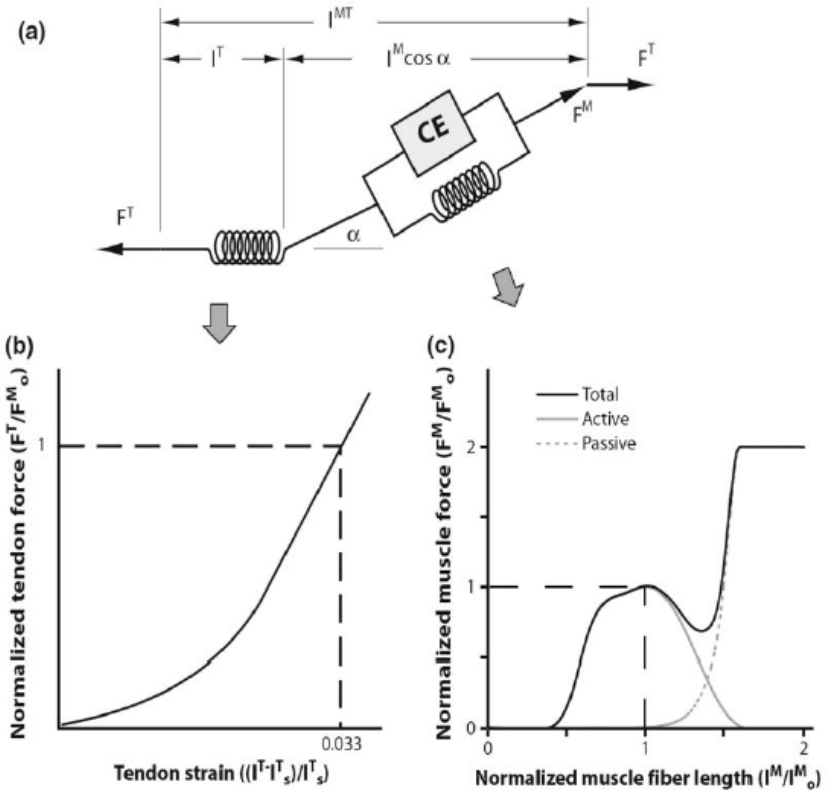

Figure 2.10: Hill's model of muscle, addapted from A Model of the Lower Limb for Analysis of Human Movement by Edith M. Arnold et al., 2010 [36].

2.3.4 Musculoskeletal model of the thoracolumbar spine

Until recently no sufficient model of the upper body comprising of the articulated thorax has been developed. The previous models have incorporated thorax as a rigid body or lacked the detailed thoracic musculature. In 2015, Bruno, Bouxsein and Anderson, using OpenSim musculoskeletal modelling software, introduced a musculoskeletal model of fully articulated thoracolumbar spine (Fig. 2.11) [34, 37]. The model comprises of individual vertebrae of the thoracolumbar spine, ribs, sternum and pelvis. Unlike the previous studies, muscle anatomy is assessed using CT data and the whole model is correlated to previous *in vivo* measurements.

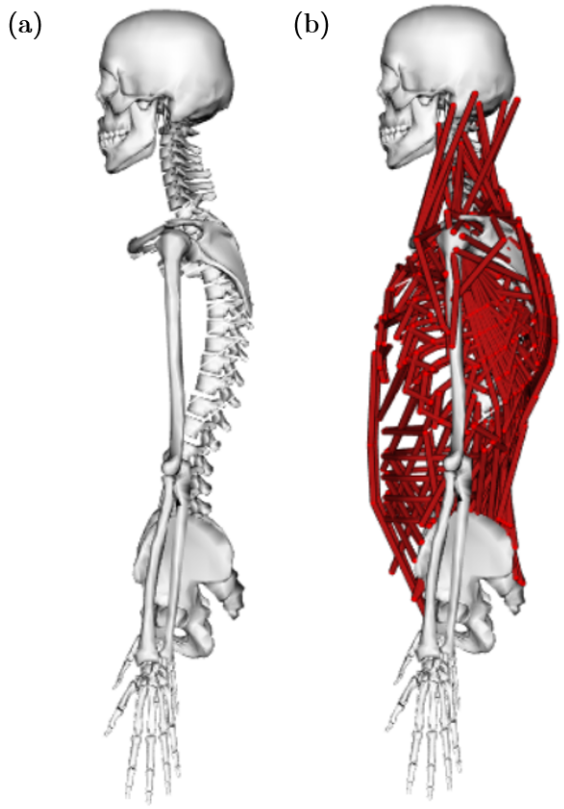

Figure 2.11: Musculoskeletal model of thoracolumbar spine made by Bruno, Bouxsein and Anderson, 2015 [37]. (a) Skeletal model, (b) complete model with muscles.

Skeletal anatomy and joints definition

The skeletal anatomy parameters were obtained from CT scans of a 25-year-old male (height 175 cm and weight 78 kg). The positions and orientations of the vertebral bodies were based on average measurements available in the literature. Thoracic kyphosis (T1-T12 Cobb angle) was set to 50° and lumbar lordosis (L1-L5 Cobb angle) set to 43°. The arms, head, and neck anatomy was taken from previously published and freely available OpenSim models (Vasavada neck model, 1998, and Stanford VA Upper Extremity model, 2005 [38, 39]).

The head and neck were then joined into a single lumped body connected to T1 (ball joint), with a single mass according to Leva, 1996 [40]. A ball joint allows three rotational degrees-of-freedom whereas pin joint provides only one rotational degree-of-freedom. The intervertebral joints (L5/S1 to T1/T2) were also modelled as ball joints. The segmental movement of the whole thoracolumbar spine is ensured in three dimensions, their centre of rotation is located at the geometric centre of the lower intervertebral disk. The model is connected to a ground through the hip joint (pin joint). The mass and centre of mass positions of body segments were based on published anthropometric ratios [40]. The mass of the trunk was proportionally assigned to the vertebral bodies and sacrum according to prior cadaver studies [40, 41]. A low mass (0.0001 kg) was assigned to ribs, sternum, clavicles, and scapulae. The mass properties of humeri, radii, ulnae and hands were adopted from the Stanford VA Upper Extremity model [39].

2.3.5 Joints and coordinates in OpenSim

Regarding the coordinate systems used in OpenSim modelling software, parent and child body need to be distinguished. A fixed parent body is located relative to the ground origin. Joints are used to define the motion of one body with respect to another, the child relative to its parent. They are located at the instantaneous axis of rotation (IAR), the point, around which the child body rotates. The *location_in_parent* sets the location of the joint in the parent body. The *location*, on the other hand, defines the position of the joint relative to the child body where it is situated. Position of the child body relative to its parents is composed of the vectors defining its origin together with two angles of rotation. One of these angles is prescribed in the .osim file as *orientation_in_parent*. It sets the orientation of the coordinate system of a child frame relative to the parent body. The second one is defined in .mot file and it describes the rotation of the child itself around IAR. How OpenSim defines a child body relative to its parent body, and about which point the transformation occurs is depicted in the picture (Fig. 2.12).

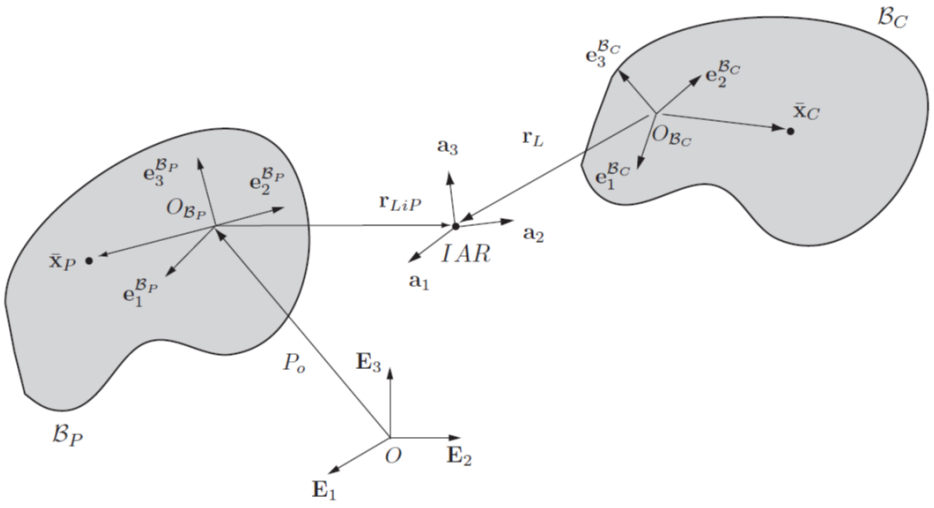

Figure 2.12: Depiction of the coordinate system used in OpenSim, adapted from A detailed open-source musculoskeletal model of the human lumbar spine by M. Christophy, 2010 [42].

A parent body is located relative to the ground origin O by P_o. The instantaneous axis of rotation, IAR, connects the parent body B_P and its child body B_C and is offset from the body fixed bases located on the parent body by the vector r_{LiP} .The child body B_C is able to spatially transform about the axes of rotation, given by a_1, a_2, a_3. The center of mass and inertia of each body are defined with respect to their body-fixed frames by the vectors x_P and x_C, respectively. Vector r_{LiP} (defined as *location_in_parent*) sets the position of IAR in the parent body while r_L (defined as *location*) specifies the position of the origin of B_C with respect to IAR.

2.3.6 Segmental angles of thoracolumbar spine in hyperextension

According to the study made by Salazar et al., 2015, the machanism of seizure-induced vertebral fractures is assumed to be the spinal hyperextension [14]. Hyperextension is achieved when the spine is in the uttermost position of its range of motion (ROM). Experiment done by Morita et al., 2014, provides data on ROM of the thoracic spine based on CT measurement of vertebral angulation during a total extension of the spine when the patient is in a laying position [43]. The values of ROM for lumbar spine were studied by Adams et al., 2013 [31]. The global angles of thoracolumbar spine in total extension are listed in the table below (Tab. 2.1).

Table 2.1: Values of global angles of thoracolumbar spine in total extension adopted from previous experiments [31, 43]. Joint description refers to the adjacent vertebrae of the articulation, excursion is angular deflection in the sagittal plane in degrees. Negative values denote to a clockwise direction.

Joint	L5/S1	L5/L4	L4/L3	L3/L2	L2/L1	L1/T12
Excursion	-6.0	8.0	18.0	25.0	28.0	26.0
Joint	T12/T11	T11/T10	T10/T9	T9/T8	T8/T7	T7/T6
Excursion	24.7	22.9	19.7	18.7	16.8	16.0
Joint	T6/T5	T5/T4	T4/T3	T3/T2	T2/T1	
Excursion	13.1	9.1	7.4	8.0	7.9	

Muscle anatomy

Muscle group is composed of multiple fascicles that generate force dependent on muscle fibre length and velocity, according to a Hill-type model of the muscle. The maximum isometric force a muscle can generate is equal to its physiologic cross-sectional area (PCSA) multiplied by a constant maximum muscle stress (MMS) [44]. Bruno, Bouxsein and Anderson, 2015, used MMS of 100 N/cm^2 for all muscles except for the shoulder muscle groups, where MMS was 140 N/cm^2.

As a small, heterogeneous group of cadavers was used to derive the PCSA and position of the muscles, the values might not be accurate and thus adjustment by *in vivo* measurement needed to be done. For those purposes, CT scans of a trunk were collected. Firstly, an equivalent muscle group PCSA and position at each vertebral mid-plane was calculated. An equivalent muscle group PCSA at the given level was obtained by summing PCSA of each fascicle of the muscle group crossing the vertebral mid-plane (Eq. 2.6).

Similarly, anteroposterior (AP) and mediolateral (ML) moment arm of the muscle group was computed by finding the centroid of fascicles at the vertebral level.

Finally, PCSA of the muscle fascicles was adjusted according to the following equation:

$$PCSA_{adj\_f} = \frac{1}{L} \cdot \sum_{i=1}^{L} PCSA_{model\_f,i} \cdot \frac{PCSA_{measured\_g,i}}{PCSA_{model\_g,i}}, \tag{2.6}$$

where $\mathrm{PCSA}_{\mathrm{measured\_g}}$ is the average PCSA of the equivalent muscle group from CT measurements, $\mathrm{PCSA}_{\mathrm{model\_g}}$ is the pre-adjusted PCSA of the muscle group in the model, $\mathrm{PCSA}_{\mathrm{model\_f}}$ is the pre-adjusted PCSA of the fascicle, $\mathrm{PCSA}_{\mathrm{adj\_f}}$ is the adjusted fascicle PCSA, and L is the number of all vertebral levels where the muscle was measured.

The attachment points of individual fascicles were then moved in the transverse plane by the difference of the measured AP and ML moment arms and the values in the model. Linear extrapolation was used to establish the data between the vertebral levels.

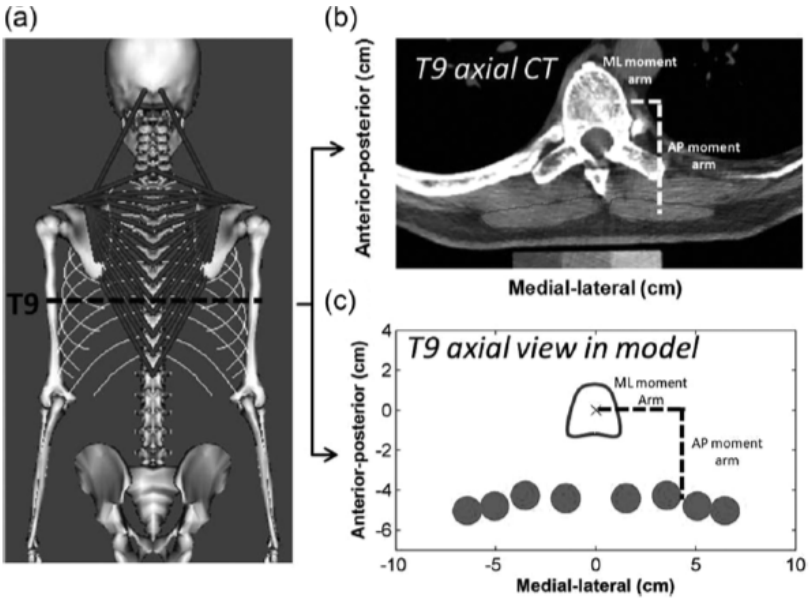

Figure 2.13: Adjustment of the muscle group attachment and PCSA. (a) The level at witch an equivalent PCSA and AP/ML moment arm are calculated (b) *in vivo* measurement from the CT scan, (c) calculation of an equivalent muscle group PCSA and AP/ML moment arm from model. Adapted from Development and Validation of a Musculoskeletal Model of the Fully Articulated Thoracolumbar Spine and Rib Cage by Bruno et al., 2015 [37].

2.4 Methods of vertebral failure load prediction

There are several studies focusing on prediction of the vertebral compressive strength evaluating the vertebral fracture risk. The ultimate strength of the trabecular bone is determined by the maximum stress carried without failure within the overall structure of the vertebral body. The trabecular bone is expected to be carrying most of the axial compressive load [45]. Previously performed studies aimed to estimate this compressive failure load by developing regression model dependent on the bone mineral density (BMD) and cross-sectional area (CSA) of the vertebral body [46, 47, 48, 49, 50]. However, study performed by Crawford, Cann and Keavenya, 2002, commented on limits of these studies as they do not take the mechanical principles into account. As they wanted to test the accuracy of these regression models, they developed a finite element model reconstructed from CT scans for compressive failure force prediction [51].

2.4.1 Regression model

Reviewing previous studies, two main strategies while predicting the vertebral fracture load based on regression models were observed. Either a new regression model correlating vertebral failure force to its CSA and BMD was developed based on an experimental measurement of cadaver specimens [48, 50, 51], or the beam theory was used to estimate the maximum force [46, 47, 49]. The second approach used experimentally developed regression model for estimation of the vertebral elastic modulus [52]. The failure load determined by these experiments across the whole population falls into a considerably wide interval (2.5-6.6 kN). A brief review of these studies follows. Studies using DXA to establish the regression model were not considered as it was found that QCT is better than DXA in clinical assessment of bone loss and fracture risk [51]. The first and the most thorough study aiming to develop the regression model for prediction of the failure load was the one performed by Brinckmann, Biggemann and Hilwegilweg, 1988 [48].

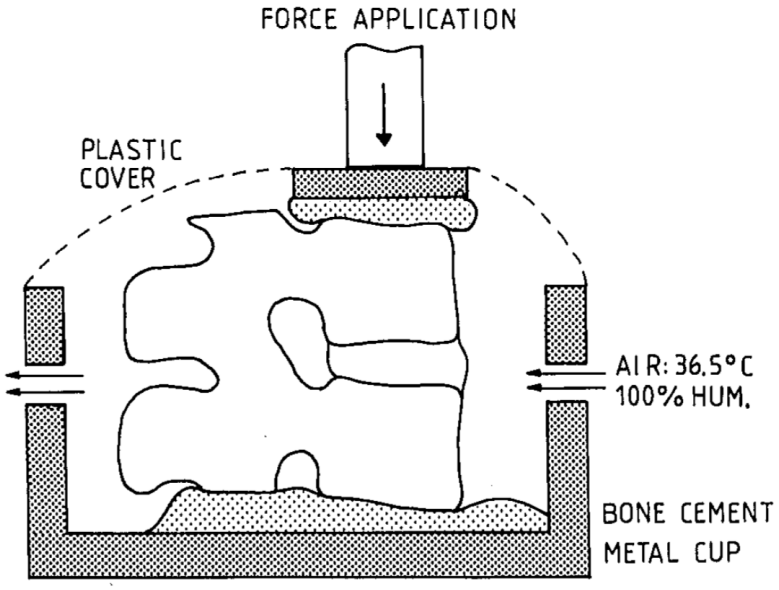

Figure 2.14: The experiment set-up of the study performed by Brinckmann et al., 1988 [48].

Experiment performed by Brinckmann et al., 1988, aimed to develop a regression model estimating the vertebral compressive failure force by conducting the measurement on 98 cadaver motion segments of human thoracolumbar spine. The veretbral compressive failure load was predicted based on BMD and CSA referring to vertebral mid-plane area measured from CT scans with an error of estimation 1 kN. The report shows an increase of the vertebral ultimate force by 0.3 kN per anatomic level in the region between T10-L5 vertebrae [48].

Brinckmann et al., 1988, based their theory on the previous finding of Hansson et al. who showed the relation between the bone mineral content and the vertebral compressive failure load. Since the dual-photon scanner was a very rare piece of equipment of the clinical institutions, the measurement of bone mineral density by dual-photon absorptiometry as Hansson suggests was not feasible. Following Hansson et al., 1980, further experiments indicated that taking geometric dimensions of the vertebrae into account leads to an acceptable estimation of the vertebral compressive failure load. As both required parameters are measurable by computed tomography, *in vivo* estimation of the vertebral failure load is possible [53].

It is generally accepted that the strength of trabecular bone increases with increasing bone density. Furthermore, at a given load, decreasing vertebral compressive stress and thus increasing load-bearing capacity is conditioned by a larger end-plate area. These phenomenons support previous studies suggesting that compressive strength of the vertebra is related to both bone density and end-plate area. Moreover, in the study made by Brinckmann et al., 1988, the Pearson's correlation coefficient is calculated for compressive failure load correlated with bone density, end-plate area and both bone density and end-plate area (0.62, 0.26 and 0.80 respectively). As the linear correlation coefficient is higher while correlating the vertebral strength with both bone density and end-plate area, it is obvious that both parameters should be taken into account [48].

To define the formula for vertebral compressive failure load calculation, mechanical testing of the cadaveric motion segments of the spine simulating *in vivo* condition was performed. The experiment included 53 specimens. During the mechanical testing, the applied load was approximately perpendicular to the disc plane (Fig. 2.14). The compressive failure load of the vertebra was defined as the force of the yield point (the force where the deformation deviated more than 0.05 mm from the straight line fitted to the linear portion of the curve). The value of compressive failure load was then measured from force-deformation curve [48].

Following the measurement of bone density and end-plate area, the equation for calculating vertebral ultimate load was derived (Eq. 2.7). The coefficients of regression was defined for various subgroups of specimens (Tab. 2.2).

$$F_U = A_0 + A_1 \cdot BMD \cdot CSA, \tag{2.7}$$

where F_U is compressive failure load in [kN], BMD is bone mineral density in [mg/ml] of K_2HPO_4, CSA is end-plate area in [cm^2] and A_0, A_1 are coefficients of linear regression.

Investigation of the end-plate area showed linear increase in the craniocaudal direction from T10-L5 by 0.5 $\pm$ 0.19 cm^2 per vertebra. Bone density showed almost constant pattern, decreasing in the craniocaudal direction from T10-L5 by 1.4 $\pm$ 2.6 mg/ml per vertebra [48].

Table 2.2: Results of the regression analysis made by Brinckmann et al., 1988.

Subgroup selected	N	A0	A1	R	SE
All specimens	98	0.32	0.00308	0.80	1.06
Male	54	0.42	0.00314	0.80	1.08
Female	44	0.45	0.00315	0.80	0.98
< 50 years	56	0.80	0.00290	0.79	1.03
> 50 years	42	0.70	0.00262	0.65	1.05
T10-L1	34	0.20	0.00301	0.84	0.88
L2-L5	64	0.59	0.00298	0.76	1.13

With the typical values of bone density 120 mg/ml, and CSA 15 cm^2, Eq. 2.7 gives the increase of compressive failure load in the anatomical level to be approximately 0.3 kN. Brinckamann et al., 1988, suggest that for an assessment of the compressive failure load of vertebrae of an individual person, only one measurement of density and end-plate area is necessary. The ultimate load of the adjacent vertebrae can be then extrapolated by adding 0.3 kN per anatomical level. This would ease the measurement and calculations as well as decrease the radiation exposure of the patient [48].

Singer et al., 1995, performed measurements on 303 isolated vertebral bodies to determine their compressive failure load experimentally. These experimental results were then correlated to trabecular bone density and vertebral cross-sectional area using quantitative computed tomography (QCT) and dual-energy X-ray absorptiometry (DXA). According to their findings, trabecular density multiplied by the midvertebral body cross-sectional area showed significant correlation with the vertebral failure load. Vertebral failure load measured in this study ranked approximately between 2.5-5.5 kN (Figure 2.15), however, regression model was not introduced. They reported the increase in the vertebral ultimate load by the vertebral level to be 0.17 kN, considerably lower than the one reported by Brinckmann et al., 1988 [48, 50].

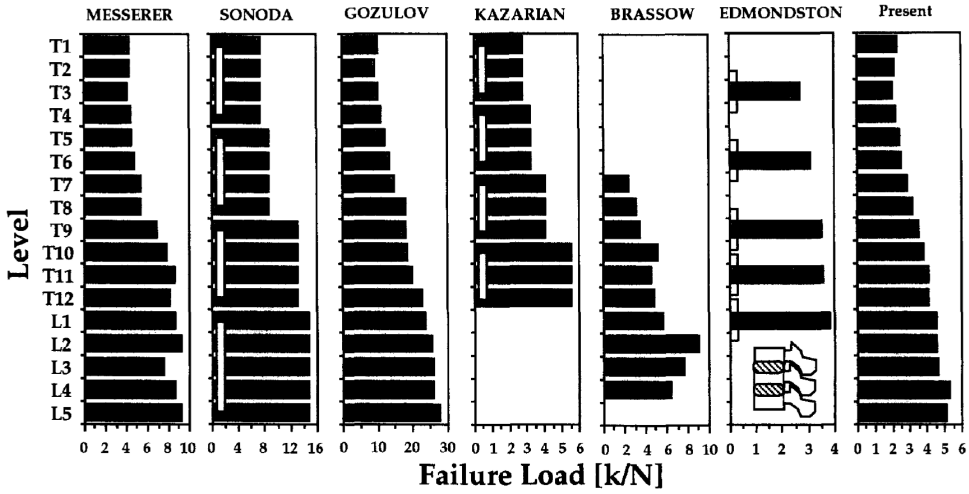

Figure 2.15: Summary of reported segmental trends in compressive failure load of isolated vertebral bodies throughout the thoracic and lumbar regions until the year of 1995, adapted from the study made by Singer et al., 1995 [50].

Kopperdahl et al., 2001, presented correlations between bone mineral density measured from CT scans and the modulus, yield stress, and yield strain of human vertebral trabecular bone by mechanical testing of cylindrical specimens of human vertebral trabecular bone (from T10 to L4) cored from 32 cadavers. They reported that bone mineral density measured from CT scans showed a strong positive correlation with elastic modulus and yield stress (r^2=0.90-0.95, p<0.001). They also reported that there was a weak positive linear correlation with yield strain ($r^2 = 0.58$, p=0.07). The principal contribution of this study was the development of a linear and power law regression models for prediction of average elastic modulus for vertebrae of the thoracolumbar spine (Eq. 2.8, $r^2 = 0.75$, p<0.05) [52].

$$E_{ave} = -34.7 + 3230 \cdot BMD, \tag{2.8}$$

where $E_a$ve is the longitudinal elastic modulus [MPa] and BMD is bone mineral density in [mg/ml] of CaHA measured from CT scans.

Bouxsein et al., 2006, followed up the study of Kopperdahl et al., 2001, by measuring the BMD and CSA of the midvertebral bodies from the CT scans of L1-L3 to compute vertebral compressive ultimate load using engineering beam theory. They assumed that bone tissue fails at a constant strain, and that the failure load for a whole bone, or its strength, is proportional to the structural rigidity at its weakest cross-section [51].

$$F_U = 0.0068 \cdot E_{ave} \cdot CSA, \tag{2.9}$$

where F_U refers to vertebral compressive ultimate load in [N], E_{ave} is vertebral average elastic modulus in z direction [MPa] and CSA is the cross-sectional area of the midvertebral body [cm^2]. The average elastic modulus (E_{ave}) in the axial direction is established according to the previously developed regression model (Eq. 2.8) [52].

Following this process of vertebral failure force estimation, values varying between 5-6.6 kN are reported for male patients across the generations (Fig. 2.16) [47].

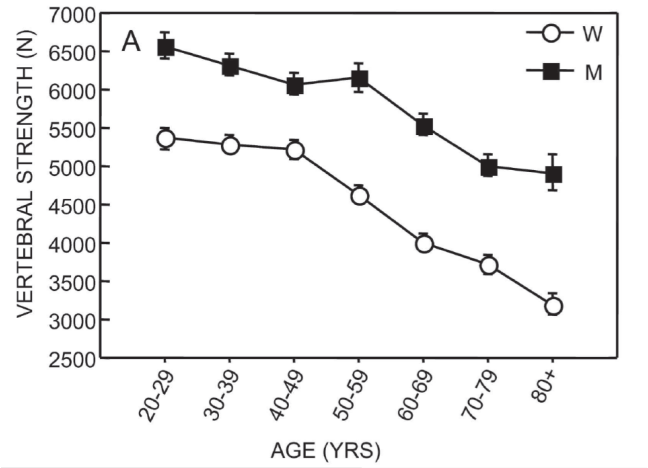

Figure 2.16: Sex and age-related vertebral failure load measured by Bouxsein et al., 2006 [47].

The same process of estimation of the vertebral failure load based on the previously published engineering beam theory followed Bruno et al., 2014, who studied sex-specific differences in skeletal fragility for 981 male-female pairs reporting the range of vertebral ultimate load 4.2-4.6 kN [49]. Bachmann et al., 2016, used the method presented by Bouxsein et al., 2006, to estimated fracture risk across the BMI spectrum for women collecting BMD and CSA of 176 women (Eq. 2.9 and 2.8). They reported vertebral ultimate load varying from 3.7 kN to 4.8 kN [46].

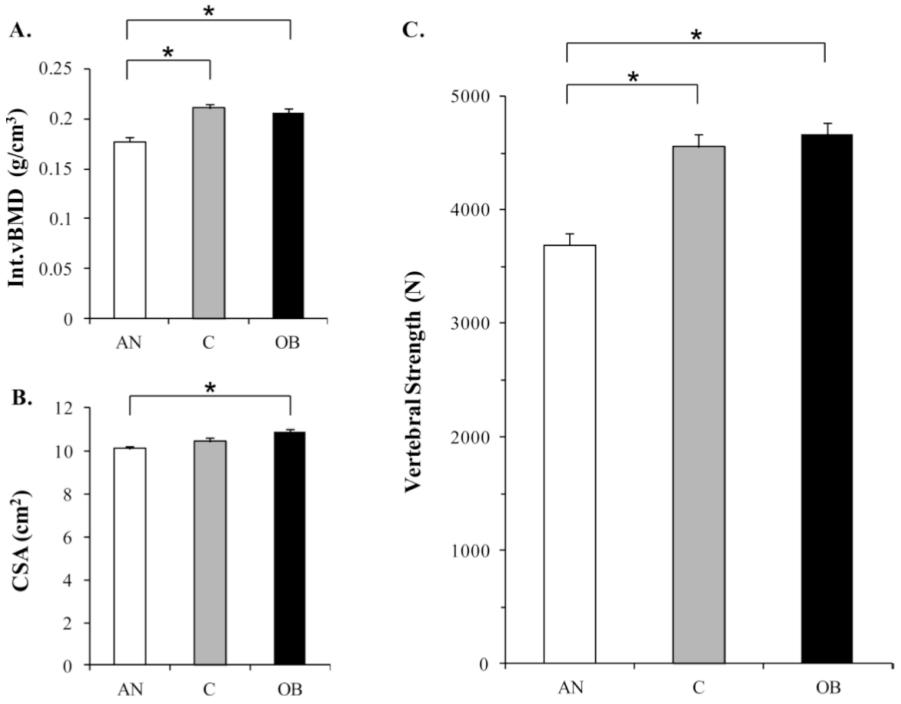

Figure 2.17: The linear combination of BMD and CSA used to estimate vertebral failure load (*p<0.004; AN, anorexia nervosa; C, lean controls; OB obese) according to Bachmann et al., 2017 [46].

	N = 981 matched pairs		
	Men	Women	
	Mean ± SE	Mean ± SE	% Diff
Unadjusted			
Cross-sectional area (cm^2)	12.39 ±0.0407	10.33 ±0.0407	20% *
Trabecular vBMD (g/cm^3)	0.137 ±0.0011	0.150 ±0.0011	–9% *
Integral vBMD (g/cm^3)	0.181 ±0.001	0.196 ±0.001	–8% *
Compressive strength (N)	4,623 ± 30	4,217 ± 30	10% *

Figure 2.18: Estimated L3 compressive failure load in men and women matched for age according to Bruno et al., 2014 [49].

2.4.2 FEM model

Using the simple regression model though, the mechanical principles are overlooked and thus the estimated compressive filure force is questioned to reflect the vertebral compressive strength. As it was previously stated, vertebral fracture results from extensive internal bone stresses and so the effects of subtle geometric features and inhomogenities of the structure may substantially affect vertebral strength. On that account, finite element model derived from QCT scans was determined to overcome such limitations [51].

The objective of the study performed by Crawford et al., 2002 , was to show that QCT-based voxel finite element models are more accurate to predict vertebral compressive strength than the regression models using BMD and CSA to assess its strength.

They used mineral density measured from CT scans of each bone voxel to define longitudinal elastic modulus values using the correlation between the elastic modulus and mineral density for vertebral trabecular bone according to the Eq. 2.8 (Fig. 2.19).

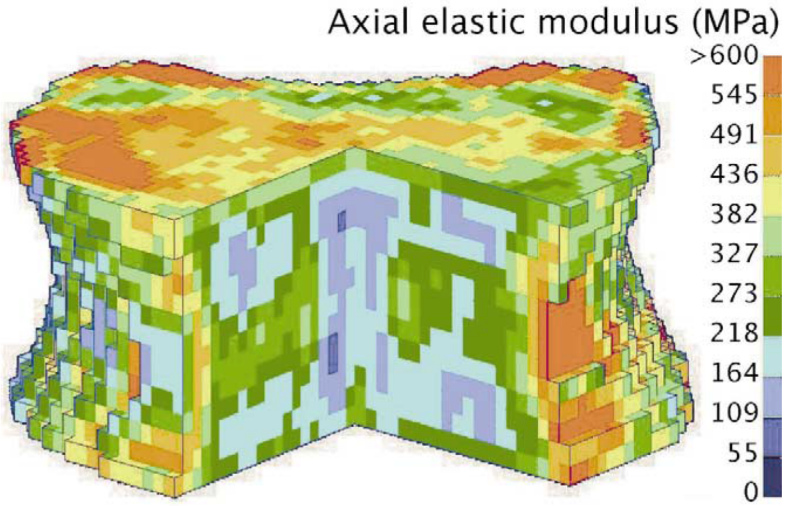

Figure 2.19: The distribution of axial elastic modulus in a voxel-based finite element model of a vertebral body used for vertebral strength estimation, adapted from the study made by Crawford et al., 2002 [51].

The remaining anisotropic engineering constants for the bone were then assigned using assumptions of transverse isotropy. Assuming that a vertebra behaves as a beam and considering the mean value of the compressive yield strain of vertebral trabecular bone ($\epsilon = 0.0077$), a linear analysis was used to compute the whole vertebral stiffness K_{FE} based on which the vertebral compressive strength was estimated:

$$F_{FE} = 0.0068 \cdot K_{FE} \cdot H, \tag{2.10}$$

where F_{FE} is vertebral compressive ultimate load estimated by FEM modelling [N], K_{FE} is the FEM stiffness in [N/mm] and H [mm] is the height of the vertebra.

Crawford et al., 2002, considered the yield strain used for the calculation of the vertebral strength as a constant value for varying bone density. Nevertheless, the positive correlation between the compressive yield strains and bulk density of the trabecular bone was shown by the study performed by Kopperdahl et al., 1998, ($r^2 = 0.52$, p=0.0002) due to a buckling mechanism of struts of the trabecular bone [54].

Within the study, vertebrae were mechanically tested in compression to measure their strength experimentally (L1-L4 vertebrae, 13 specimens). When comparing experimentally measured vertebral failure load in compression, positive correlation was found with the theoretical vertebral strength estimated by FEM modelling ($r^2 = 0.86$, p=0.0001). As expected, the vertebral failure load established as a product of BMD and vertebral minimum CSA (r^2=0.65, p=0.0008), and BMD alone ($r^2 = 0.53$, p=0.005) shows smaller coefficient of determination that the one estimated by FEM modelling. The findings are, that the-FEM derived vertberal strength estimation is more accurate although regression models are statistically significant [51].

2.4.3 Assessment of bone mineral density from CT scans

In order to predict the vertebral ultimate load, assessment of vertebral BMD is required. It is possible to establish patient-specific BMD of individual vertebrae by *in vivo* measurement on CT scans. BMD, however, cannot be measured directly from CT scans. From CT scan, Hounsfield units (HU) of the tissue are measured and then converted to the corresponding BMD [55].

HU are usually converted to BMD by means of phantoms, the rods containing given concentrations of mineral (CaHA or K_2HPO_4). If phantoms cannot be used, phantom-less calibration can be performed as well. Weaver et al., 2015, proposed a method to establish BMD in mg/ml of CaHA from linear regression model. Linear regression model between the measured HU units and unknown BMD is established from a set of equations (Eq. 2.12) of the known BMD of fat and muscle and corresponding HU of the tissue measured from the CT scans [56].

$$-69 = k \cdot HU_{fat} + q \tag{2.11}$$

$$77 = k \cdot HU_{muscle} + q, \tag{2.12}$$

where -69 mg/ml of CaHA is the BMD of fat, HU_{fat} is CT value of fat, 77 mg/ml of CaHA is BMD of muscle and HU_{muscle} is CT value of muscle.

Proposed phantom-less calibration takes account of specific parameters of CT scanner. However, no studies on phantom-less calibration of BMD in mg/ml of K_2HPO_4 were found. Cann and Genant, 1980, developed a regression model based on which HU can be calibrated to vertebral BMD in mg/ml of K_2HPO_4 (Eq. 2.13) [57].

$$BMD_{K2HPO4} = 0.77 \cdot HU - 2.17, \tag{2.13}$$

where BMD_{K2HPO4} is bone mineral density in mg/ml of K_2HPO_4 and HU is the mean value of Hounsfield units of the measured area.

2.5 Summary of the literature review

Literature review revealed that although being rare, there are more cases of seizure-induced vertebral fractures which were not caused by any external trauma. The fractures were reported to be located at the level of thoracic or lumbar spine. Although a cause of fracture was attributed to a strong paraspinal muscle stretch, the theory has not been confirmed and fracture mechanism not explained. It is assumed that during an epileptic seizure, back muscles develop the force exceeding the vertebral ultimate load causing the bone to break. To support this hypothesis, forces acting on each vertebra during the seizure as well as vertebral failure force of individual vertebrae has to be estimated.

Epileptic seizure presents an extreme case which goes againts the normal physiological conditions and so musculoskeletal models cannot be used for vertebral compressive forces estimation. However, the nature of the studied case might have an affect on the redundancy of the problem. Considering the muscle stretching maximally during the seizure, muscle forces are no longer unknown and so the problem becomes determinate. So as to establish the total compressive force acting on each vertebra, the equilibrium-based model can be used. As an input parameters, isometric forces of selected muscle groups as well as the direction of their action lines have to be established. Additional parameter required for further calculations is the orientation of the given vertebra. Vertebral orientation determines perpendicular direction to the vertebral body and thus the compressive component of the total force. The musculoskeletal model developed by Bruno et al., 2012, presents a suitable tool for the assessment of these parameters. Regarding the complexity of the analysis, MATLAB MathWorks will be used for follow-up computations as well as data selection and evaluation for estimation of vertebral compressive load during the seizure.

It was found that patient-specific failure load of vertebrae can be simply predicted by correlation to its CSA and BMD. For those purposes, multiple regression models allowing *in vivo* prediction of the vertebral ultimate load were developed. In order to use the regression models, vertebral cross-sectional area together with its bone mineral density (BMD) have to be measured from patient's CT scans. As calibration rods are not present on the patient's CT scans, regression model-based or phantom-less calibration has to be used to convert the measured HU to vertebral BMD.

Chapter 3

Thesis objective

It is assumed that even in the absence of external trauma, the extreme muscle stretch may result in vertebral fractures. Yet this hypothesis is not very well accepted as the muscle stretch is often disregarded to be strong enough to break such a solid structure as the bone. To broaden the awareness of this potential risk of misdiagnosis, analysis of the case of an epileptic patient providing the computational background to support the hypothesis needs to be performed. The hypothesis might be supported by prediction of vertebral failure load and its comparison to the extreme intersegmental compressive forces induced by the back muscles during the seizure. The objective of the thesis and the outline of the individual steps which have been made to accomplish these targets follow.

Thesis outline

- **Hypothesis:**
  An extreme stretch of back muscles can result in vertebral compressive fracture
- **Thesis objective:**
  Estimate the risk of vertebral body fracture during epileptic seizure based on patient-specific biomechanical analysis
- **Specific aims:**
  1. Estimation of compressive force acting on each vertebra of thoracic spine
     (a) Computational model definition
     (b) Parameters assessment
     (c) Muscle selection
     (d) Equilibrium equations formulation
     (e) Estimation of intersegmental compressive force acting on each vertebra
  2. Prediction of compressive vertebral failure load of individual vertebrae
     (a) Vertebral body cross-sectional area measurement
     (b) BMD assessment
     (c) Vertebral ultimate load prediction
  3. Comparison of the predicted vertebral ultimate load and estimated forces compressing the individual vertebrae

Chapter 4

Methods

In this chapter, the process of prediction of vertebral compressive failure load of each vertebra as well as estimation of intersegmental forces acting perpendicular to the vertebral body will be described.

4.1 Vertebral compressive force estimation

Forces acting on the spine include not only the muscle force and body weight, but also tension in the spinal ligaments and surrounding tissue, intraabdominal pressure, and any applied external loads. Given by the nature of the case this thesis is investigating, no external loads and intraabdominal pressure will be considered. Furthermore, tension in the spinal ligaments will be neglected. In summary, the aim is to estimate force acting perpendicularly on each vertebra of thoracic spine generated by back muscles and the body weight which satisfy single-level equilibrium. This force will then be compared to the vertebral compressive failure load predicted based on the previous experiment.

4.1.1 Computational model definition

It should be noted that the spinal biomechanics presents a complex problem and thus the computational model needs to be greatly simplified. Not only are the physiological conditions of the patient in the seizure unknown but also the musculoskeletal model providing the parameters for further calculations has already been developed and sets certain limitations. Regarding the physiological conditions of the patient in an epileptic seizure, the position of the patient as well as the magnitude of forces acting on the spine have to be defined. However, these parameters are not given precisely and they need to be estimated. While calculating the total force acting on the vertebra, several essential assumptions were adopted.

The case of an epileptic patient which was being analyzed was modelled as a static problem of an upper body being held in extension, while the major back muscles of the spine developed their maximal isometric forces. It was assumed that the patient stopped breathing during the seizure and thus the intraabdominal pressure was not considered. Furthermore, even distribution of the compressive force on the vertebral body was presumed without considering any disc degeneration.

1. Thoracolumbar spine is in total extension
2. Intraabdominal pressure is not considered
3. Only major back muscles are taken into account
4. Muscles stretch with their maximal isometric force
5. Compressive force acting in the mid-plane of the disc is transferred evenly onto the vertebral body

4.1.2 Parameters assessment

Parameters needed for further calculation included muscle attachments, muscle force directions and maximal isometric forces of each muscle group. Furthermore, locations of joints between individual vertebrae had to be determined as the equilibrium equations were then calculated at the level of intervertebral joints. Global coordinates of joints together with the muscle attachment locations were also needed for assessment of the forces of the selected muscle groups on the individual vertebrae. Last but not least, vertebral orientation in the given position of the patient had to be determined so as to decompose the resultant force to its compresssive component.

The process of obtaining this data is described in more details below. All of these parameters were established using musculoskeletal model of the fully articulated thoracolumbar spine and rib cage made by Bruno, Bouxsein and Anderson, 2015, previously presented in Chapter 2 which was incorporated in OpenSim modelling software [37, 34]. The required parameters are listed below:

1. Muscle parameters
   (a) Muscle attachments
   (b) Muscle force directions
   (c) Maximal isometric forces of the muscle groups
2. Skeletal parameters
   (a) Global coordinates of the joints
   (b) Vertebral orientations

Patient-specific scaling of the model

The model incorporated in OpenSim modelling software can be scaled to the patient's body weight or more precisely, the scaling can be based on motion analysis of the specific patient. During motion analysis scaling, locations of markers are obtained using motion capture equipment. For the purposes of this study, the model was simply adjusted to the patient's body weight of 70 kg. Value of 47 kg was set for the weight of the upper body representing 68.2% of the whole body weight [58].

Motion setup

Prior to the asssessment of parameters required for further calculation, motion file which set the model into the desired position needed to be created. The position in which the body is modelled is important not only for the global location of bones and their articulations but also for muscle attachments positions and directions in which the forces are applied.

The total spine extension seems to be the most relevant to the position of the spine during the tonic phase of an epileptic seizure. It is assumed that spinal muscles during a seizure were stretched maximally and deflected the spine into its extreme position. To simulate the posture of the thoracolumbar spine in a seizure, the vertebral joints excursion is set to the uttermost position of their range of motion in spinal extension. The angular excursion of the joints prescribed in the motion file was held constant.

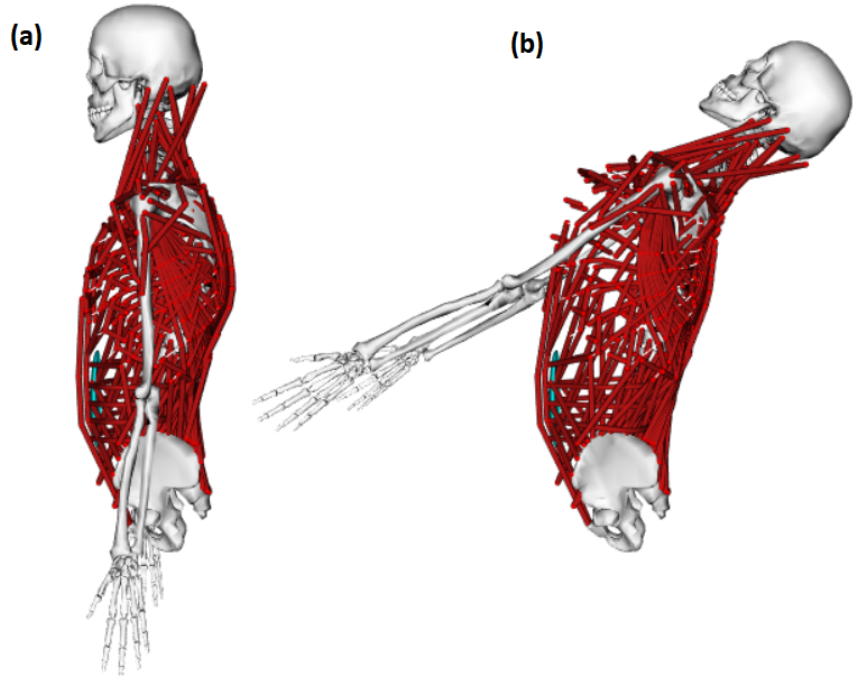

Figure 4.1: Musculoskeletal model in the neutral position and in the full extension of the thoracolumbar spine. (a) Neutral position of the body, (b) total extension of the thoracolumbar spine.

The angles obtained from these studies represent global angles of the vertebrae. These angles refer to the global angles of the vertebrae in the neutral position summed up with the motion angles of a total extension (4.2). The imput data of motion angles are then defined as follows:

$$\alpha_n = \beta_n - \beta_{n-1} - orientation\_in\_parent_n; n =< 2, 17 >, \tag{4.1}$$

where n=2 refers to L4 and n=17 refers to T1, α_{n} is a motion angle of the n-th vertebra, β_{n} is a global angle of the n-th vertebra, $\beta_{\mathrm{n-1}}$ is a global angle of the previous vertebra and *orientation_in_parent* is the orientation of joint assigned to the n-th vertebra in its parent body ((n-1)-th vertebra).

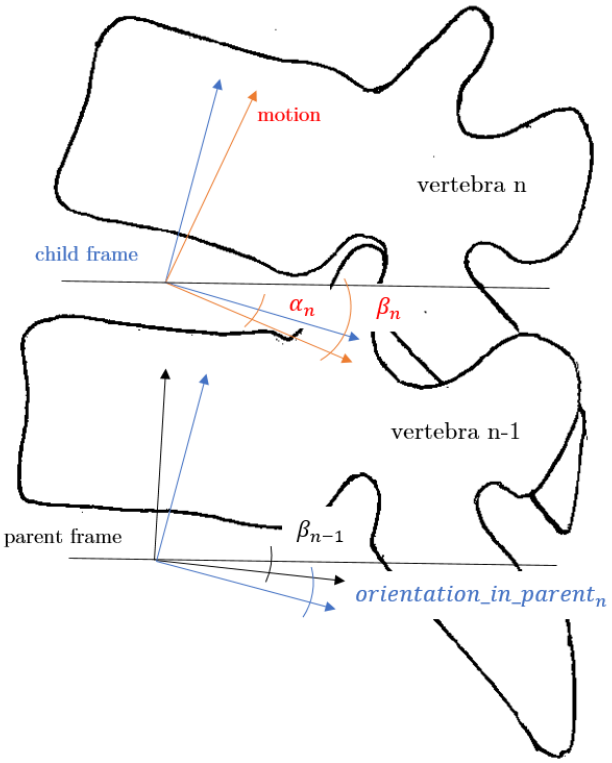

Figure 4.2: Illustration of angles between two adjacent vertebrae in OpenSim modelling software.

For the first vertebra in a cranial direction (L5), Eq. 4.1 is simplified:

$$\alpha_1 = \beta_1 - (-21), \tag{4.2}$$

where α_1 is a motion angle of L5 with respect to the sacrum, β_1 is a global angle of L5 and -21° is *orientation_in_parent* of the joint L5-S1 as the sacrum is already orientated in the ground directions [37] .

Motion angles of intervertebral segmental movement for thoracolumbar spine in total extension are presented in Chapter 2 (Tab. 2.1). After loading the motion file into musculoskeletal model in OpenSim, the model took position as depicted in Fig. 2.11).

Muscle parameters

There are three parameters of muscles required for further calculation. (1) Muscle force attachment, that is the origin and insertion of muscles, fully determining location of the muscle. (2) Muscle force direction which affect the contribution of each muscle group to the resulting vertebral compressive force. (3) Maximal isometric force of each muscle group.

Files containing muscle force direction and muscle attachment were generated from the musculoskeletal model using OpenSim plugin made by Luca Modenese [59, 60]. The plugin included an analysis called *MuscleForceDirection* that allows the user to extract the attachment positions and lines of action of the muscles attached to the selected bodies for a given kinematics. Given an appropriate musculoskeletal model, the plugin allows to extract following parameters:

1. The muscle attachment positions
2. The muscle force directions

MuscleForceDirection_vectors.sto output file contains the normalized vectors representing the directions of the muscle lines of action. The vector is always pointing from the selected body where the attachment is located outwards.
MuscleForceDirection_attachments.sto include the coordinates of the muscle attachments. Both the attachments and the muscle force directions can be expressed in the ground or in the segment reference frame.

To be able to run the analysis, motion file had to be loaded into the model first. Both parameters, muscle force direction and muscle attachment, were obtained in global reference system. Maximal isometric forces of each muscle group were extracted from the musculoskeletal model as well, directly from the source file of the model (Appendix B).

Skeletal parameters

In OpenSim, instantaneous axis of rotation, IAR, provides the location of the joint connecting the parent body and its child. It is offset from the body fixed bases located on the parent body by *location_in_parent*. One way of collecting global coordinates of the joints is by summing the location of IAR on parent body and the global location of the parent body itself. However, as the parent body is a child of another adjacent vertebra, its global coordinate is not given directly and *location_in_parent* and *location* along all of the previous vertebrae have to be summed up.

Regarding the difficulty of the method, an alternative method was developed. The method includes creation of imaginary muscles having their origin in one vertebral junction and their ending in an adjacent one. As the previously described MuscleForceDirection analysis allows to export global coordinates of the muscles at any position set by the motion file, muscles with no isometric forces can be used to establish the joint locations in ground reference system without affecting the model kinematics. Imaginary muscle connecting each vertebral joint were thus prescribed into the .osim file of the model. Their isometric force was set zero. After loading the motion file, MuscleForceDirection analysis was carried out and the location of vertebral joints in global coordinates were then extracted.

4.1.3 Muscle selection

Musculoskeletal model of thoracolumbar spine used for analysis included 32 muscle groups consisting of 552 fascicles. Prior to the analysis, these muscles had to be sorted so as only the major back muscles were included in the analysis. As intraabdominal pressure was not considered, abdominal muscles are supposed to have minimal effect on the spine. Furthermore, arms are allowed to move freely and thus no force of the muscles of upper extremities are applied to vertebrae. Number of muscle fascicles involved in the analysis was so reduced to 308. The groups of selected muscles are shown in the Figure4.3.

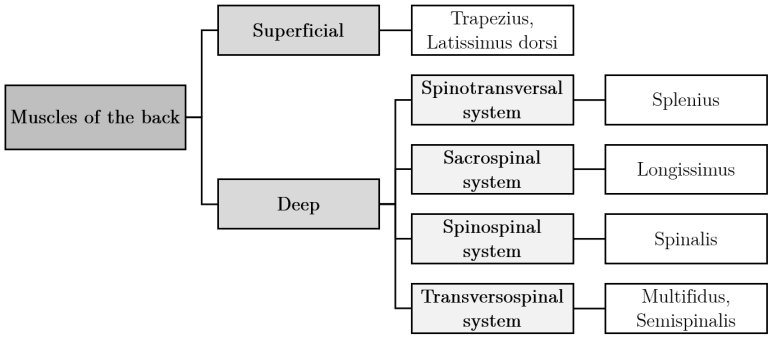

Figure 4.3: Muscle groups selected to be compressing spine during an epileptic seizure.

4.1.4 Equilibrium equation formulation

Before the equilibrium equations were formulated, the affect of the muscles on each vertebra needed to be assessed. It was supposed that muscles compress the vertebra only if its proximal attachment was located above and its distant attachment below the vertebra. So as to decide which muscle is affecting the given vertebra, global coordinates of the joints, as well as the global coordinates of the muscle attachments had to be extracted from the musculoskeletal model. Global locations of the vertebral joints as well as muscle attachments were first imported into MATLAB and vectors of their y-coordinates were created. To determine whether the individual muscle fascicle has an impact on a vertebra, a loop comparing vertical attachment position of the muscle to the y coordinate of the vertebral joint was used (Eq. 4.3). This way, a matrix of zeros and units is created having 18 rows referring to vertebral joints and 308 columns corresponding to muscle fascicles (m_10, Eq. 4.4). Zero was assigned to the field referring to the muscle of the specific column with no affect on the vertebra of the specific row.

$$if\ y_{1,j} > y_i \wedge y_{2,j} < y_i \rightarrow muscle\ j\ has\ impact\ on\ vertebra\ i \tag{4.3}$$

$$for\ i-th\ vertebra,\ muscle\ j \begin{cases} has\ no\ impact & : M_{10}(i,j) = 0 \\ has\ impact & : M_{10}(i,j) = 1, \end{cases} \tag{4.4}$$

where i=<1,12> refers to individual vertebrae of thoracic spine (T1-T12), j=<1,308> defines the muscle group, $y_{1,j}, y_{2,j}$ are y-coordinate of attachement of the muscle j, y_i is y-coordinate of the joint and m_10 is the matrix of ones and zeros.

Once the impact of each muscle group on specific vertebra (T1-T12) was determined, the direction it is acting in as well as its force needed to be included into calculations. File containing muscle force direction extracted from the model by means of previously mentioned MuscleForceDirection analysis was loaded into MATLAB. Maximal isometric forces of muscle groups were generated from musculoskeletal model and imported into MATLAB as well. Matrix of zeros and units according to whether the muscle compresses the vertebra or not (m_{10}) was then multiplied by a vector of muscle forces in x and y direction (Eq. 4.5, 4.5).

$$F_x(i,j) = m_{10}(i,j) \otimes F_{iso}(j) \otimes n_x(j) \tag{4.5}$$

$$F_y(i,j) = m_{10}(i,j) \otimes F_{iso}(j) \otimes n_x(j) \tag{4.6}$$

where i=<1,12> refers to individual vertebrae of thoracic spine (T1-T12), j=<1,308> defines the muscle group, m_{10} is the matrix of ones and zeros, $F_x(i,j)$ is x component of the force of j-th muscle fascicle acting on vertebra i, $F_y(i,j)$ is y component of the force of j-th muscle fascicle acting on vertebra i and $n_x(j), n_x(j)$ is x and y coordinates of unit vector defining the fascicle direction, $\otimes$ refers to element-wise multiplication.

By summing up the forces in x and y direction acting on individual vertebrae, the resultant force at each thoracic level was determined, i.e. total force on the vertebra in the sagittal plane in x and y global coordinates (Eq. 4.7).

$$F_x(i) = \sum_{j=1}^{308} F_x(i,j), \quad F_y(i) = \sum_{j=1}^{308} F_y(i,j), \tag{4.7}$$

i=<1,12> refers to individual vertebrae of thoracic spine (T1-T12), j=<1,308> defines the muscle group, $F_x(i)$ is vertical force acting on i-th vertebra, $F_y(i)$ is horizontal force acting on i-th vertebra, $F_x(i,j)$ and $F_y(i,j)$ are defined previously.

Finally, so as to establish the force perpendicular to the vertebral body, resultant force was transformed into the local coordinate system of the given vertebra by means of rotation matrix (Eq. 4.8). Angle of rotation along the z axis referred to the vertebral global orientation. The component in y local coordinate system is the force compressing the given vertebra.

$$\begin{bmatrix} F_S \\ F_c \end{bmatrix} = \begin{bmatrix} cos(\beta) & -sin(\beta) \\ sin(\beta) & cos(\beta) \end{bmatrix} \cdot \begin{bmatrix} F_x \\ F_y \end{bmatrix}, \tag{4.8}$$

where F_c is the force perpendicular to the given vertebra, F_S is the shear force in posterior direction, F_x and F_y are the components of the resultant force in global coordinate system and β is the rotation angle.

4.2 Vertebral failure load prediction

The compressive failure load of the given vertebra needs to be predicted in order to come to the conclusion whether compressive forces working on the specific vertebra might result in the vertebral fracture. It is a challenging task to determine the load under which the vertebra fractures. The bone is a complex living tissue and its mechanical response should not be assessed according to one mechanical property. However, for the purpose of this study, the approximate analysis will be adopted. The aim is to estimate compressive force produced by the musculature under extreme conditions and compare it to the load threshold of the thoracic vertebrae of the specific patient. With the required parameters obtained from the musculoskeletal model made by Bruno et al., 2015, and further calculations, the total compressive force on each vertebra of the lower back was determined.

According to the study made by Brinckmann et al, 1988, the compressive failure load of thoracolumbar vertebrae can be predicted from bone density and end-plate area of the vertebral body. The method allows to predict the vertebral mechanical properties *in vivo*. And therefore, it is convenient for analysis of the clinical case. Apart from regression model developed by Brinckmann et al., Crawford's regression model was used for analysis as well. Furthermore, the approach proposed by Bouxsein et al., predicting the failure load based on vertebral average elastic modulus with the use of beam theory was implemented.

Regression model used for prediction of vertebral failure load is described in Chapter 2 (Eq. 2.7, Tab. 2.2). As this study aims to predict the compressive filure force of thoracic vertebrae of the male patient, coefficients determined for all specimens, only male cadavers and thoracic vertebra were used for calculation. The coefficients established by Crawford et al., 2003, are: $A_0 = 25.6$ and $A_1 = 806$. Model for vertebral failure load prediction proposed by Bouxsein et al., 2006, is based on estimated average elastic modulus according to Kopperdahl et al., 2002 (Eq. 2.9, Eq. 2.8). For all of these models, vertebral BMD and CSA of each vertebra of the thoracic spine must be measured from CT scans first. CT scans were obtained with sagittal and coronal reconstruction using multi-slice spiral unit, with 2 mm thickness.

4.2.1 Assessment of bone mineral density

Bone mineral density (BMD) is the amount of a certain mineral in a volume of bone tissue. One way of how to establish this value is by *in vivo* measurement based on the quantitative computed tomography (QCT). Values of the CT scans, Hounsfield units (HU), are strongly related to density of biological tissues and thus can be used for establishment of mineral density of the bone. A special attention should be payed to a mineral based on which the BMD is assessed. Brinckmann et al., 1988, correlated their model to BMD given in mg/ml of K_2HPO_4 which differs from the commonly used BMD in mg of CaHA, which was used while developing the regression model for average vertebral elastic modulus by Kopperdahl et al., 2001 [52].

Within the study, the CT values were measured over a fixed area of the trabecular bone of each vertebra of the thoracic spine in order to establish the mean value. Mean value was subsequently converted to BMD based on CaHA content by means of phantom-less calibration described in the study made by Weaver et al., 2015 [56]. Following Cann and Genant, 1980, HU were calibrated to BMD in mg/ml of K_2HPO_4 as well [57].

The process of establishment of vertebral BMD in mg/ml of K_2HPO_4 included four steps. (1) The mean values of HU units of each vertebra of the thoracic spine were measured. The ellipse surrounding the area of interest needed to be created far enough from the cortical bone. The measurement was performed in the mid-plane area in the transverse plane. (2) The mean value of HU of the chosen muscle as well as area of fat was measured so as to establish the regression model. (3) Regression model created from the given set of equations was established (Equation 2.12). (4) Mean values of HU measured for each vertebra of thoracic spine were converted to BMD in mg/ml of CaHA.

To calibrate mean HU measured from patient's CT scans to vertebral BMD in mg/ml of K_2HPO_4, previously established regression model was used (Eq. 2.13) and only step (1) and (4) was performed. The resulting regression model for establishment of BMD in mg/ml of CaHA was derived from the set of linear equations (Eq. 2.12):

$$BMD_{CaHA} = 0.91 \cdot HU + 31.38, \tag{4.9}$$

where BMD_{CaHA} is bone mineral density in mg/ml of CaHA and HU is the mean value of Hounsfield units of the measured area.

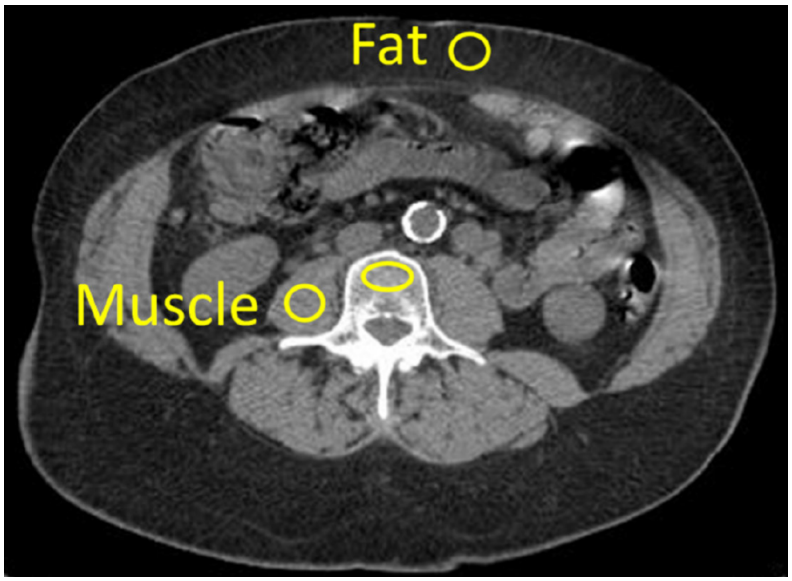

Figure 4.4: Measurement of mean values of HU of muscle tissue and fat used for phantom-less calibration.

4.2.2 Measurement of vertebral mid-plane area

Cross-sectional area of each thoracic vertebra was determined analytically from the measurement performed in the transverse plane and the angle of vertebral orientation. Vertebral mean cross-sectional area was established from ten measurements in the transverse plane using ImageJ, Java-based image processing program developed at the National Institutes of Health [61, 62]. As CT scans provide either sagittal, frontal or transverse views of the spine, the measurement was performed in the transverse plane. Ten measurements at each thoracic level were performed (Fig. 4.5). Once the angle between the transverse plane and vertebral midplane was measured from the sagittal view of the CT scans, vertebral midplane area was analytically established by multiplication of the measured value by cosine of vertebral angulation.

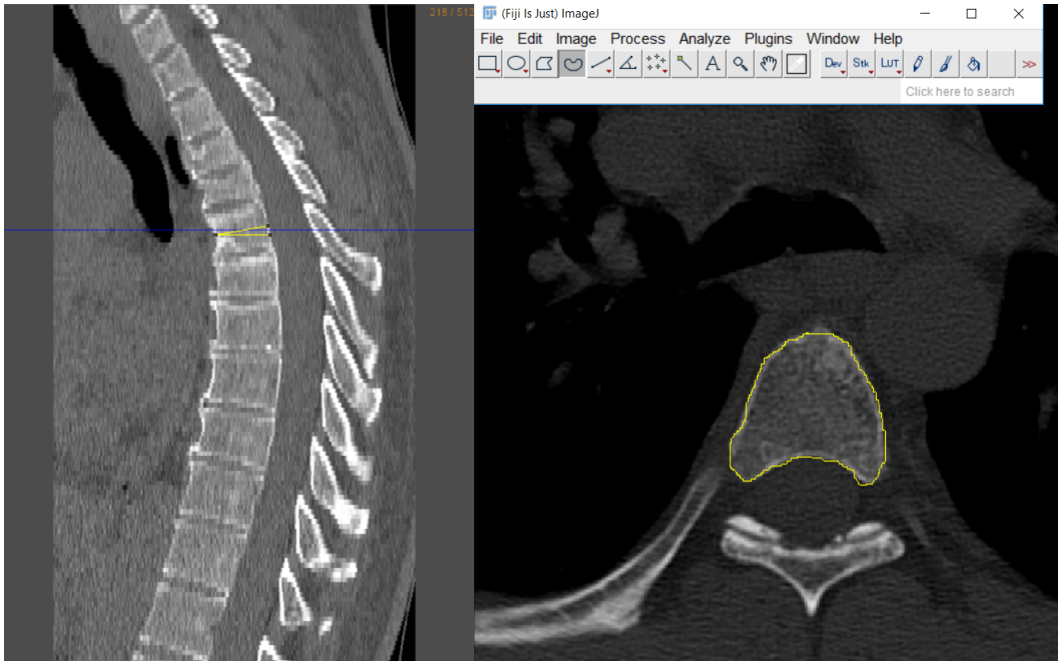

Figure 4.5: Measurement of the vertebral cross-sectional area and orientation in the transverse plane performed in ImageJ.

Chapter 5

Results

5.1 Main results

It was found that at certain vertebral levels the compressive force may exceed the vertebral failure load (Fig. 5.1). These findings support the initial hypothesis (Chapter 3) that compressive vertebral fracture can indeed be caused by muscle contraction.

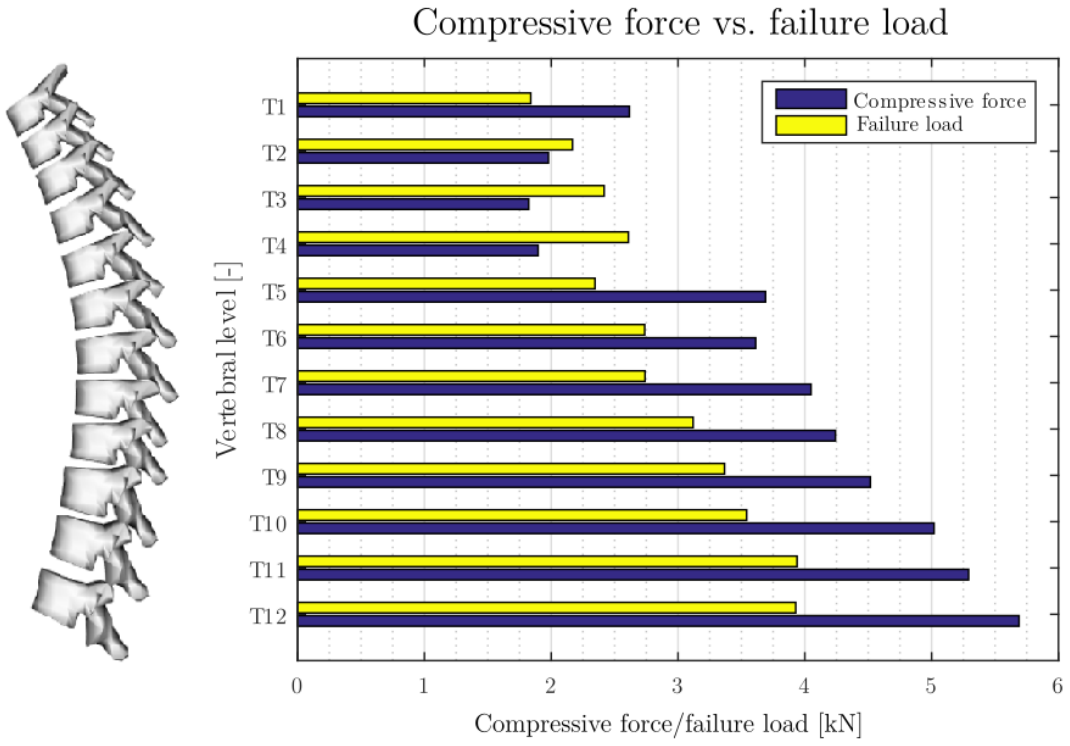

Figure 5.1: Comparison of the maximal compressive force induced by the back muscles and body weight on each vertebra of the thoracic spine and estimated ultimate load of the given vertebra. Vertebral failure load was predicted according to Brinckmann et al., 1988, with the use of regression coefficients for thoracic vertebrae [48]).

Generally, compressive force tends to increase caudally (Fig. 5.1). Nevertheless, this does not apply to the upper part of the spine (T1-T4) where the sudden drop in the force can be observed. In the region from T2 to T4, the force compressing vertebrae is lower than the vertebral ultimate load and from T5 it subsequently begins to rise above.

The gradual rise in compressive force could be explained by the increase in body weight in the inferior direction. However, the increment of the force caused by the body weight with each vertebral level is negligible (Fig. 5.2).

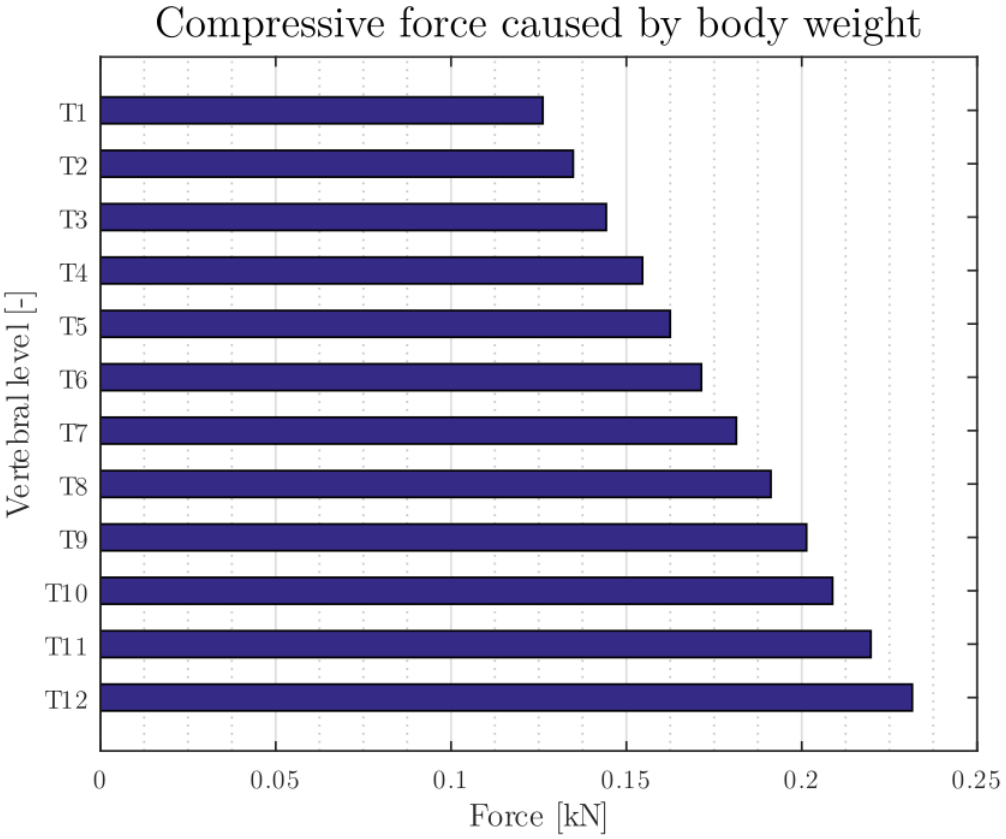

Figure 5.2: The component of the total compressive force given by the weight of the body part located above the vertebra.

The increase, and most importantly, sudden steps in compressive force development might be explained by further analysis of the back muscles compressing the given vertebra. The fifth thoracic vertebra (T5) will be taken as an example. The muscle groups selected to be compressing T5 vertebra are depicted in Fig. 5.3. In the case of T5, the major contribution to the resultant compressive force show erector spinae muscles and latissimus dorsi (Fig. 5.4, see the red and blue line). As these muscles present the strongest back muscles, higher density of their fascicles at the T5 level results in the large increase in the total force compressing the veretbra.

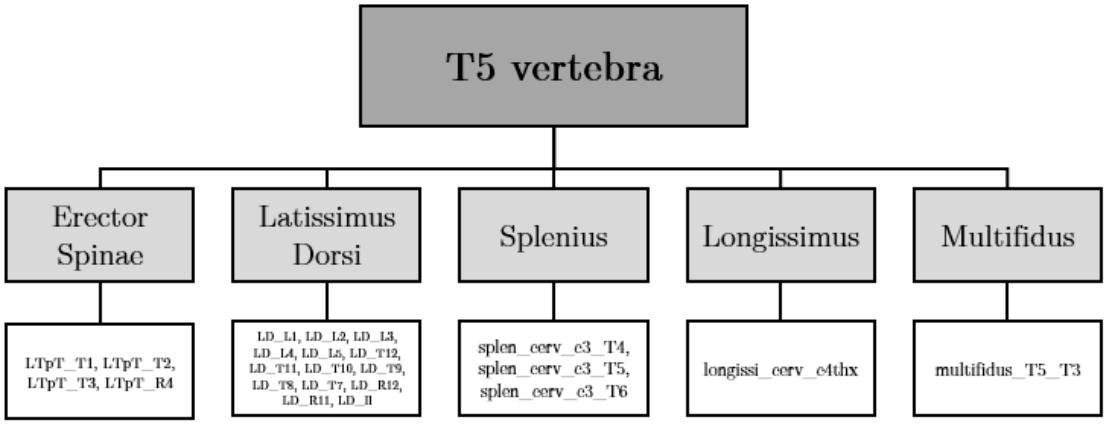

Figure 5.3: Muscles groups and their fascicles selected to be compressing the fifth thoracic vertebra (T5).

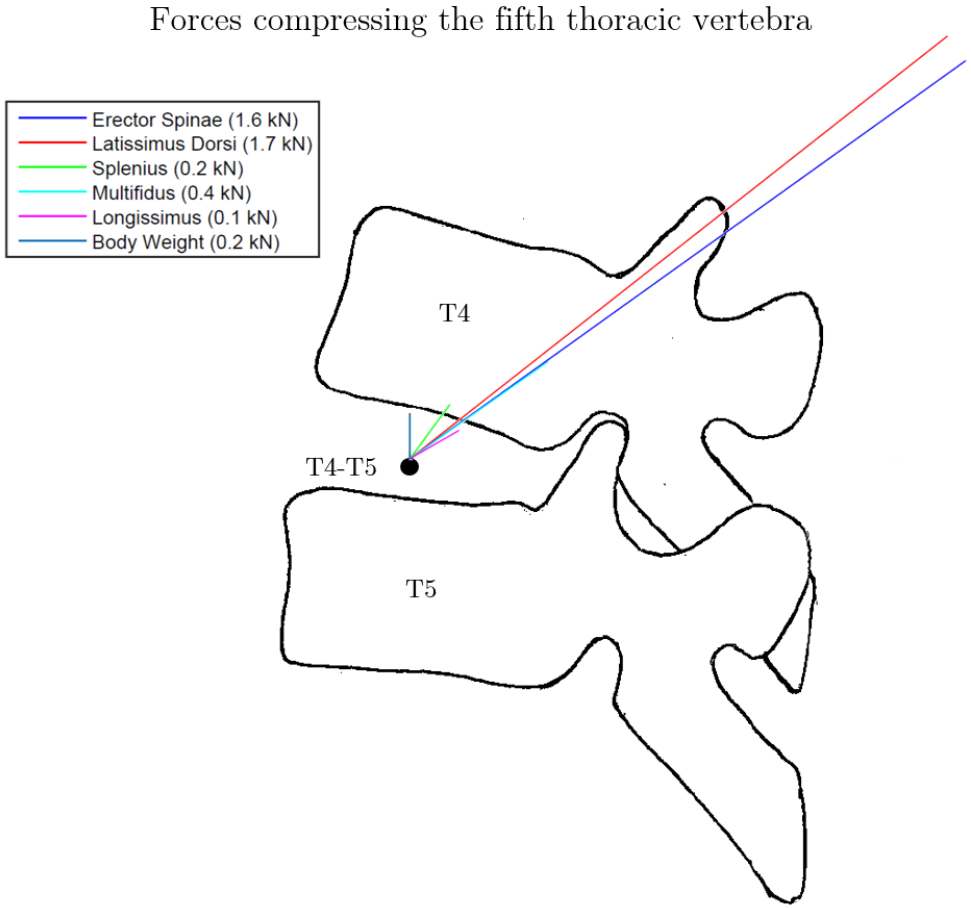

Figure 5.4: Sagittal view of the muscle forces and body weight contributing to the resultant compressive force applied to vertebra T5.

Such as the force compressing the vertebrae, the ultimate load of vertebrae increases downwards the spine (Fig. 5.1). On account of enlargement of the vertebral cross-sectional area in the inferior direction, increasing tendency of the vertebral strength was expected. The pattern of the vertebral strength follows the development of the measured vertebral area (Fig. 5.10). The lower the vertebral position, the larger the vertebral cross-sectional area. On the contrary, the BMD value is rather constant and thus does not influence the progress of the vertebral compressive strength significantly.

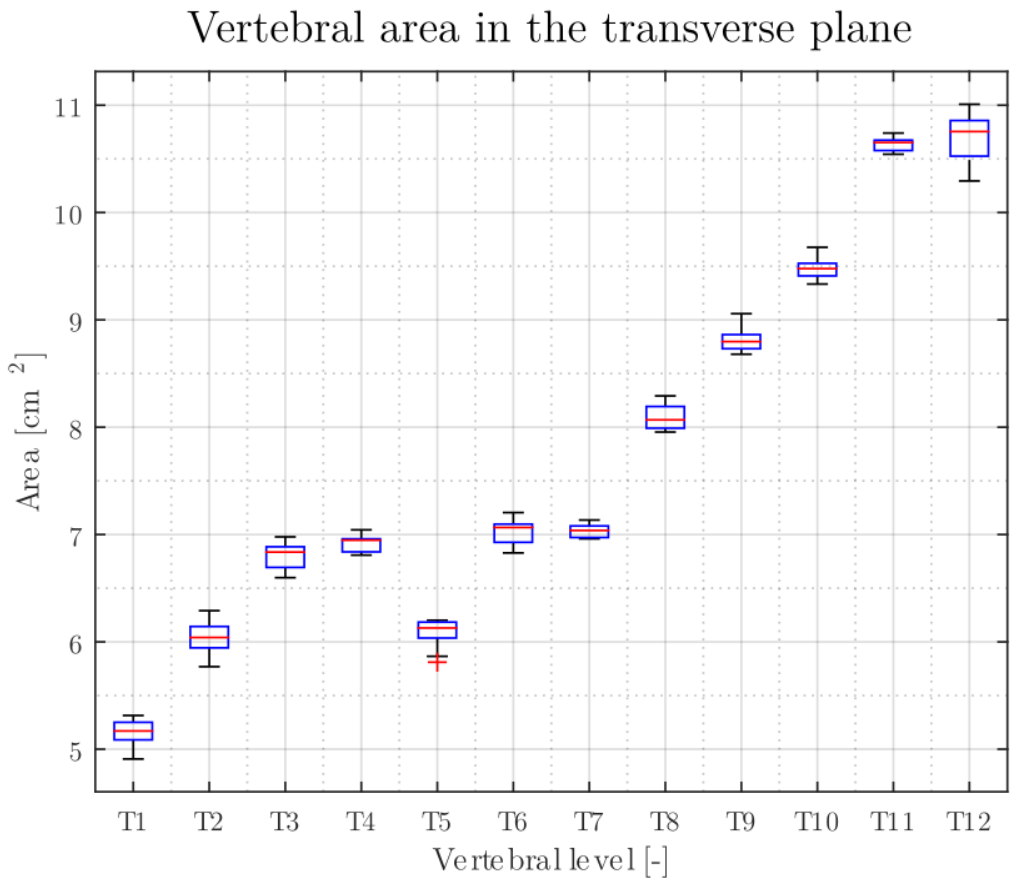

Figure 5.5: Vertebral cross-sectional area measured in the transverse plane.

To estimate maximal load that can be carried by vertebrae, methods proposed by Bouxsein et al., 2006, Brinckmann et al., 1988, and Crawford et al., 2003, were used (Fig. 5.6). Whereas the regression model presented by Bouxsein et al. gives slightly lower values of the failure load, estimation based on Brinckmann's and Crawford's models is very similar.

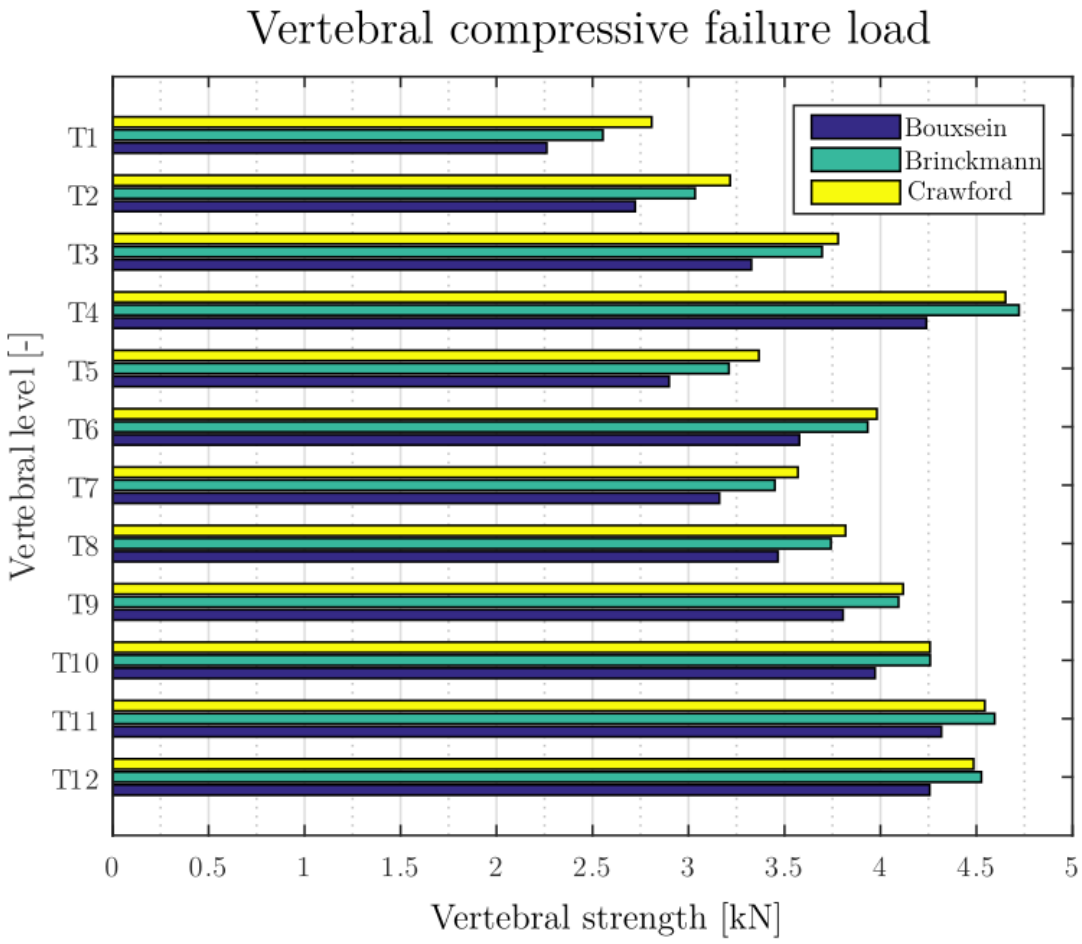

Figure 5.6: Prediction of vertebral failure load based on three different regression models with the use of BMD measured from the patient's CT scans.

However, there are many possible combinations of the input values of Brinckmann's model. Different coefficients of the linear regression using BMD from measurement done by Brinckmann et al., 1988, were considered to establish the least favourable combination. The ultimated load of each vertebra was calculated with regression coefficients representing (1) all of the specimens of the experiment, (2) only male cadavers and (3) thoracic spine region with BMD 0.12 g/ml K_2HPO_4 and (4) regression coefficient determined for thoracic vertebrae with BMD determined from patient's CT scans (Figure 5.7). The lowest vertebral strength, determining the most extreme case, was calculated using the coefficient assigned to thoracic vertebrae and mean BMD proposed by Brinckmann et al., 1988.

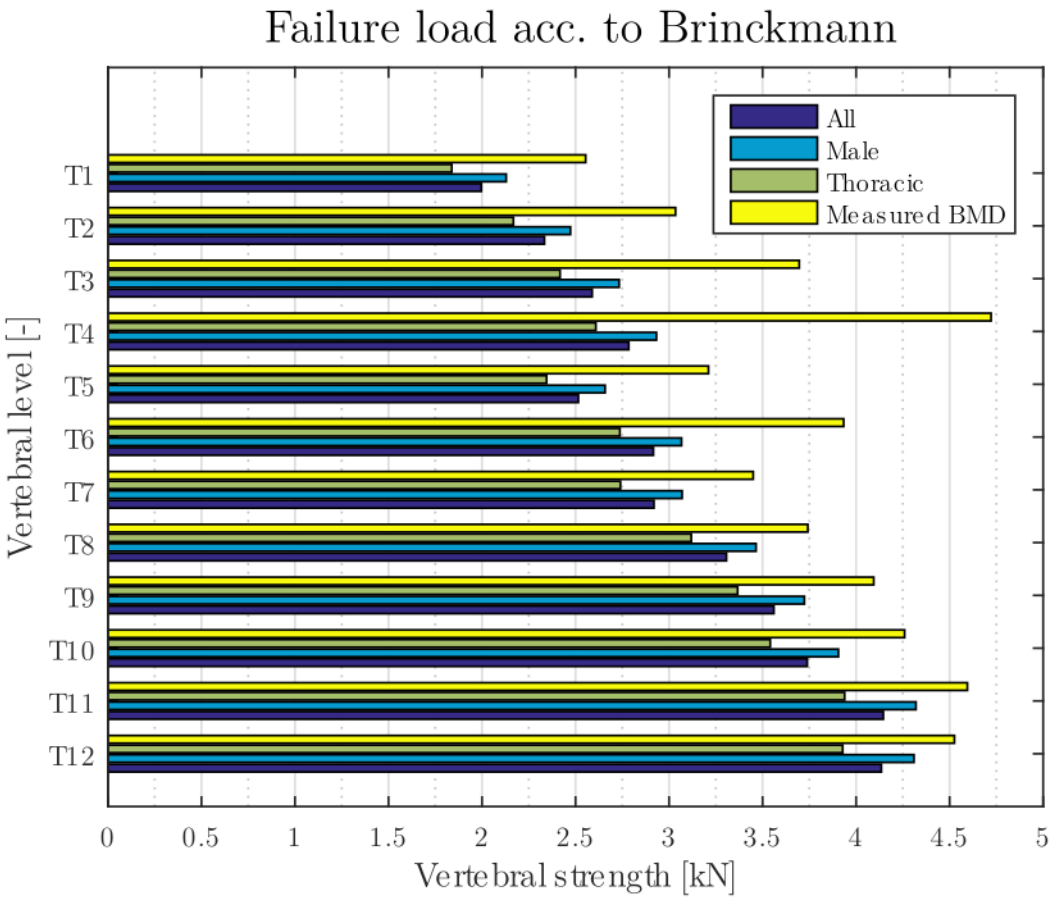

Figure 5.7: Vertebral strength estimated based on different regression coefficients and measured BMD.

5.2 Minor results

There are several minor results leading to the previously discussed principal findings. These results are presented in the following section. The section is divided into the subsection related to compressive muscle force determination and the part regarding the vertebral failure load estimation.

Compressive force

The motion angles prescribed in the motion file are listed in Tab. 5.1. Global coordinates of the vertical locations of the vertebral joints were then established incorporating the imaginary muscles into the musculoskeletal model. These values determine the transverse planes in which the resultant force is subsequently determined (see Appendix A).

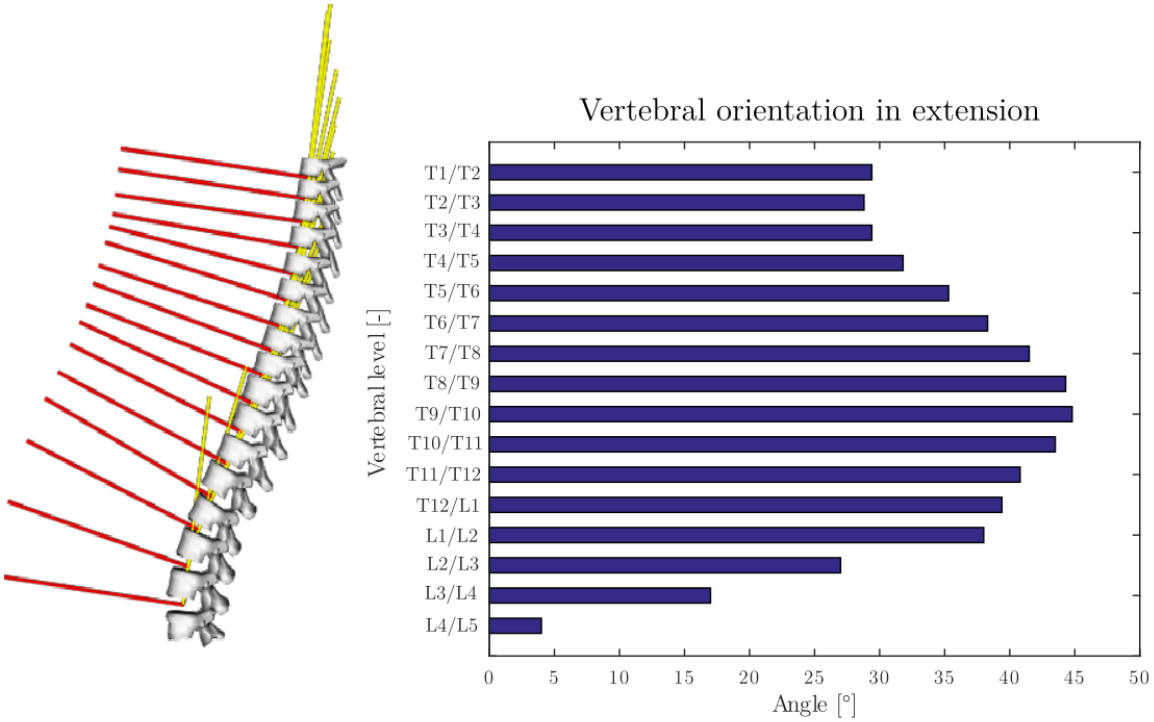

Figure 5.8: Global orientation of individual vertebrae in total extension.

Given the previously stated assumptions (page 38), only the back muscles are supposed to be compressing the spine during an epileptic seizure and thus the fascicles comprised in the model had to be eliminated. The muscle fascicles selected to be involved in further analysis are listed in Appendix B together with their physiological parameters.

The resultant force, produced by the body weight and active forces of the back muscles, compressing each vertebra was calculated for the whole thoraclumbar spine (Fig. 5.9).

Table 5.1: Values of motion angles which were prescribed in the motion file setting the model into the desired position. Negative values denote to a clockwise direction.

Joint	L5/S1	L5/L4	L4/L3	L3/L2	L2/L1	L1/T12
Excursion [°]	15.0	-4.0	-2.0	0.0	-3.0	0.0
Joint	T12/T11	T11/T10	T10/T9	T9/T8	T8/T7	T7/T6
Excursion [°]	2.7	3.2	0.8	4.0	4.1	5.2
Joint	T6/T5	T5/T4	T4/T3	T3/T2	T2/T1	
Excursion [°]	3.1	2.0	2.3	3.6	0.9	

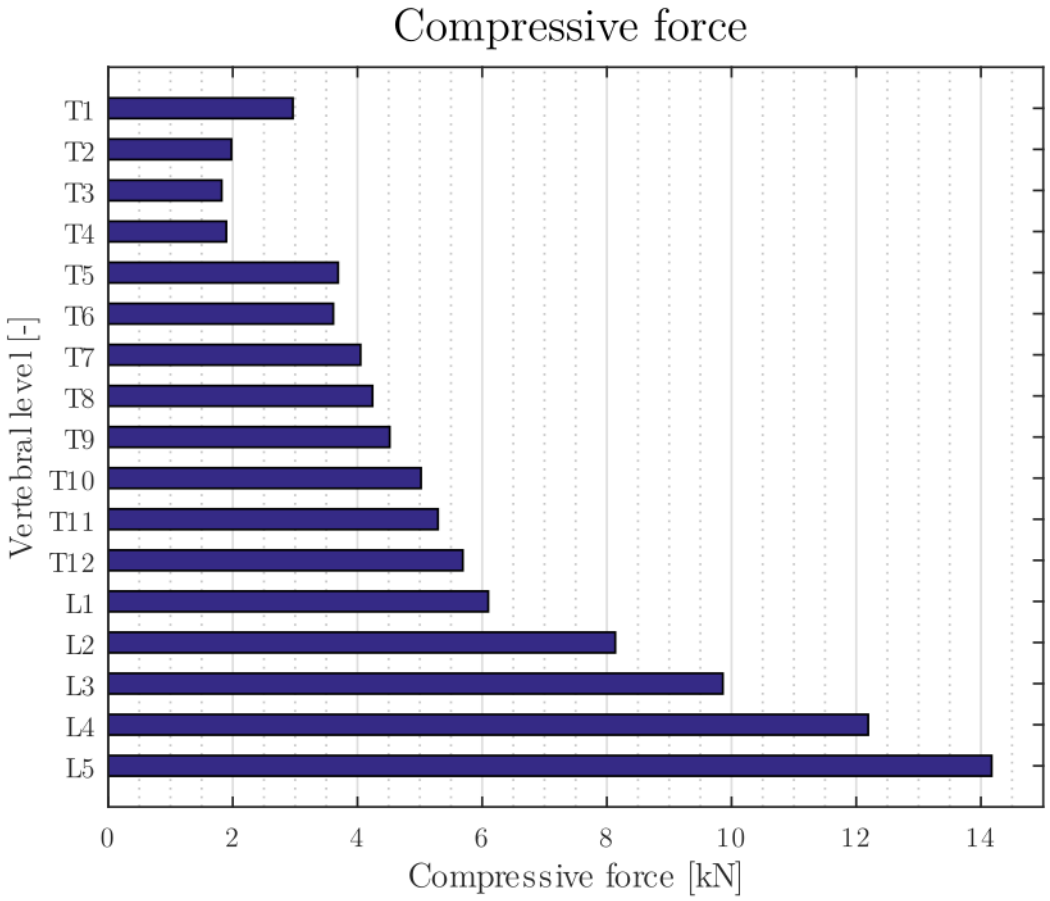

Figure 5.9: The resultant force induced by back muscles and body weight.

Vertebral failure load

Cross-sectional area of the vertebral mid-plane is increasing caudally and ranges between 6.25 and 10.2 cm^2 (Fig. 5.10).Vertebral angles measured relative to the transverse plane were used for establishment of the vertebral mid-plane area (see Appendix C).

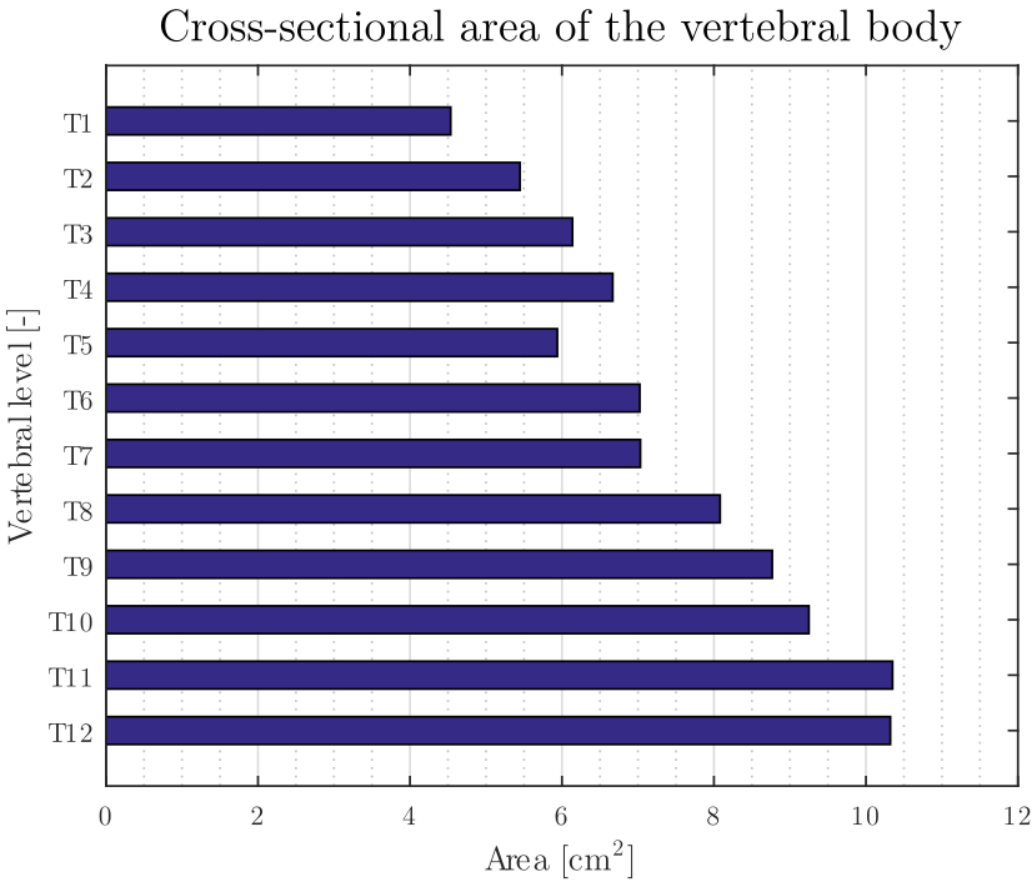

Figure 5.10: Vertebral mid-plane area established analytically from the area measured in the transverse plane.

Further measurements on CT scans included determination of HU of the vertebral trabecular bone. The mean values of HU were then converted to the BMD in g/ml of K_2HPO_4 by means of calibration base on regression model (Fig. 5.11). Mean value of BMD across thoracic vertebrae is 0.17 g/ml of K_2HPO_4.

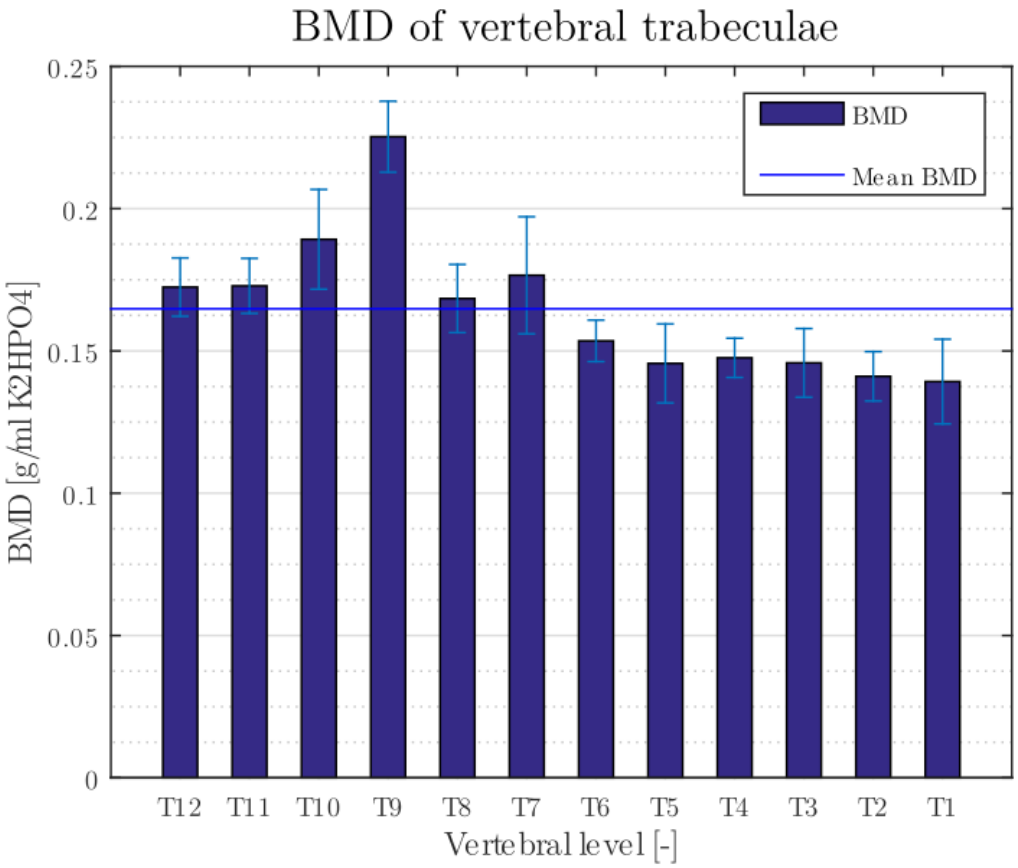

Figure 5.11: Mineral density of trabecular bone of each thoracic vertebra measured from patient's CT scans specified in grams of K_2HPO_4/ml.

Chapter 6

Discussion

6.1 Compressive forces on vertebrae

Estimated compressive force of the back muscles, assuming their maximal stretch, ranges from approximately 2 to 14 kN but does not exceed 6 kN for the thoracic part of the spine. These values are considerably higher than the forces excerted on vertebrae in spinal extension under normal physiological conditions, reported to be approximately 0.7 kN [30]. The estimation even exceeds the higher loads during daily life activities measured by instrumented implants which might reach up to 1.7 kN [28].

Regarding the progress of the estimated compressive forces across the spine, there is a visible increase in the compressive force at T5 vertebral level (Fig. 5.6). This sudden step can be explained when investigating the muscles acting on spine. At T5, not only do the fascicles of erector spinae become much denser at this level but also the number of fascicles of latissimus dorsi increases. Consequently, the force compressing T5 is much higher than the one applied to T4.

For estimation of compressive spinal loads during the sizure, simplified model had to be defined. Epileptic seizure was modelled as a static problem when the spine was held in an extreme position of its range of motion (hyperextension) and the back muscles stretched maximally. No dynamic effect of the body mass on the resultant compressive force nor the kinematics of the muscle fibres was included into analysis.

There is no doubt that the body weight and skeletal magnitude play their roles in spinal compressive loads estimation. Hence, for patient-specific analysis, musculoskeletal model had to scaled to the patient's anatomical parameters. OpenSim allows to scale the model according to the patients's upper body weight and so the model was adjusted to the value corresponding to the total body weight of 70 kg. It was assumed that the upper body weight ammounts to 68.2% of the whole body weight [58]. However, there is no need for high precision as the contribution of certain muscle groups to the total force compressing vertebrae is several times higher than the contribution of the body weight.

Parameters more important for estimation of compressive spinal loads are the forces developed by individual fascicles during the seizure. Muscles are supposed to stretch maximally during a tonic phase of an epileptic seizure. However, no studies providing a further description of muscle forces developed during the seizure were found and thus the muscles were assumed to excert their maximal isometric force. These values were taken over from the musculoskeletal model made by Bruno et al., 2015 (Appendix B) [37]. In the model, the values from previous studies were adjusted according to the CT scans of a 25-year old man. As the subject of this study is a man at the age of 45 of a similar weight, it was assumed that maximal isometric forces of the muscles are comparable. However, the muscles of the older man might be stronger resulting in even higher spinal loads.

The maximal isometric force is enduce when the activation signal from the central neural system to the muscles is maximal, a=1, assuming the optimal length of the fibres while producing the force. However, according to the results of this study, for some vertebrae, the predicted failure load might be reached even without the maximal muscle activation. Taking the fifth thoracic vertebra as an example, activation of individual muscle fascicles required for development of the force equivalent to the vertebral ultimate load was evaluated (Fig. 6.1). For those purposes, optimization minimizing the total muscle activation was performed. It was found, that although latissimus dorsi have the greatest contribution to the total compressive force, the strength of its individual fascicles is not fully employed (a<0.5). Assuming lower maximal isometric forces of multifidus or erector spinae, the ultimate vertebral load can still be reached by higher activation of fascicles of latissimus dorsi which can considerably increase the force compressing the vertebra.

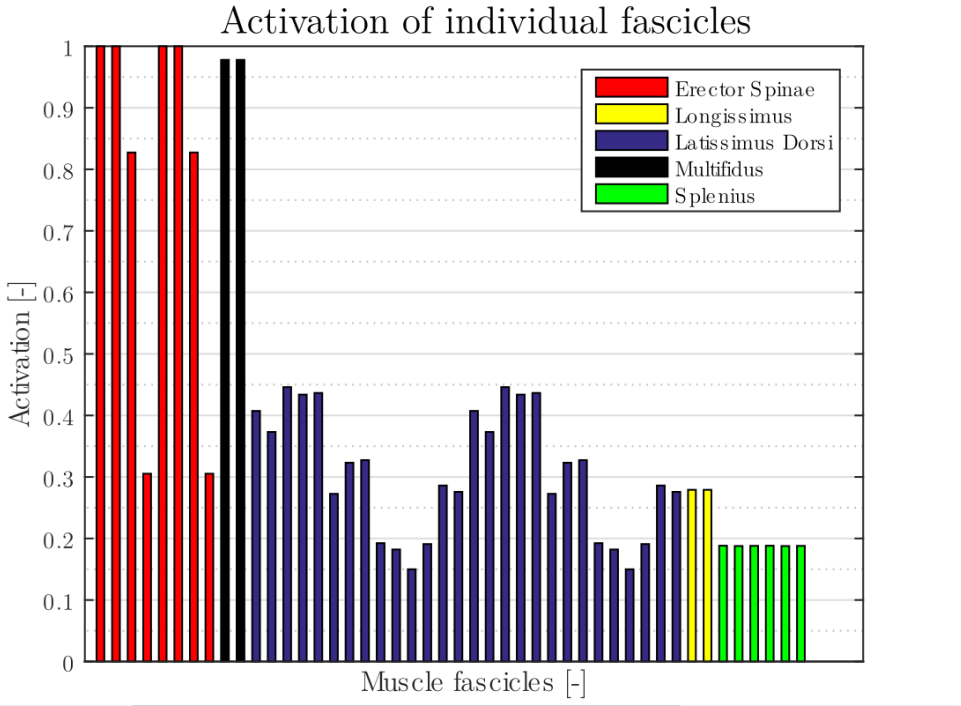

Figure 6.1: Activation of individual fascicles compressing the fifth thoracic vertebra necessary to develop force equivalent to the vertebral ultimate load.

As for the muscles incorporated in the analysis, the coplexity of the problem was reduced by taking only the back muscles into account. The force of passive structures of the anterior part of the spine were neglected as their contributon was regarded to be small when compared to the maximal muscle stretch. Morover, an impact of abdominal muscles on the spine is believed to be mediated through the abdominal pressure and diaphragm and thus they were not considered to have any significant effect on the spinal compression. Abdominal pressure is an important variable in musculoskeletal analysis. However, during a tonic phase of an epileptic seizure, a patient is supposed to exhale and stop breathing and so the abdominal pressure was not involved in the analysis.

So as to investigate the similarity of the patient's skeletal parameters to the musculoskeletal model, the global vertebral orientations in an upstand position were compared. In most cases, the modelled angles follow the curvature of the patient's spine well (Fig. 6.2). However, at the T6, T7 and T12 level, there can be a slight difference observed.

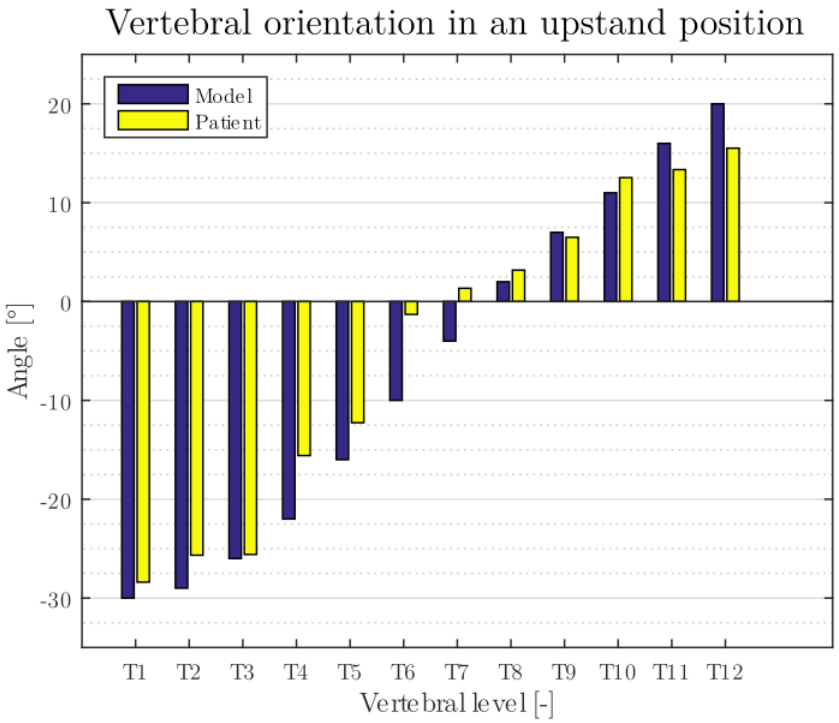

Figure 6.2: Comparison of the modelled spine curvature (global vertebral angles) and the curvature of the patient's spine.

It was a difficult task to define patient's body position during the seizure. No previous studies on angular excursion of individual vertebrae during seizure have been found and so the estimation based on a common observation had to be done. A tonic phase of a seizure is described as a sudden extreme contraction of the musculature resulting in hyperextension of the whole body. To determine the position of the thoracolumbar spine during seizure, the individual vertebrae were thus set to the uttermost position of their ROM in extension.

6.2 Vertebral failure load

In this study, the lowest mean compressive failure load of patient's thoracic vertebrae, 2.9 ± 1 kN, representing the most extreme case, was predicted by regression model made by Brinckmann et al., 1988, with the use of reported mean BMD, 120 mg/ml of K_2HPO_4. Values calculated based on other regression models with the use of BMD measured from patient's CT scans were slightly higher, 3.5 ± 0.5 kN, 3.8 ± 1.1 kN and 3.9 ± 1.1 kN (Bouxsein, Brinckmann and Crawford respectively). All of the predicted failure loads fall into the lower part of the interval reported in the literature (2.5-6.6 kN) [47, 49, 51, 52, 50]. As the increase in the failure load by vertebral level is reported to be 0.17 kN [50], it is possible that the first thoracic vertebra withstands approximately 3 kN lower load than the last lumbar vertebra.

Among all of the approaches to vertebral failure force prediction, FEM modelling of vertebra presented by Crawford et al., 2002, provides without any doubt the most precise and accurate prediction. In this study, the mechanical principals were used to estimate the external compressive force resulting in vertebral fracture by creating QCT-based voxel FEM model to predict the vertebral strength, accounting for the vertebral inner inhomogenities and anisotropy. On the other hand, as the external muscle forces on the vertebra during en epileptic seizure cannot be established accurately and a lot of simplifications must be introduced, simple regression model seems to be sufficient for vertebral fracture load prediction.

Some of the studies considered engineering beam theory to predict the vertebral fracture load using the average elastic modulus estimated by linear regression model developed by Kopperdahl et al., 2001. This technique might have an advantage over the other studies as the elastic modulus estimation is better correlated to *in vitro* measurements, however, failure force of the vertebra estimated using predicted elastic modulus together with the beam theory lacks the experimental varification.

All of the three regression models used for vertebral fracture load estimation, either incorporating the beam theory or providing only the statistical prediction, provided similar results (Fig. 5.6). As expected, progress of the failure load across the spine followed the development of vertebral cross-sectional area. Difference between the results did not exceed 1 kN which is a comparable value with the error of estimation of each regression models (Brinckmann et al, 1988, reported error of 1 kN).

However, BMD which is greatly affecting prediction of vertebral ultimate load was considerably lower when measured from patient's CT scans than the one reported by Brinckmann et al., 1988. They reported mean BMD of thoracic vertebrae to be 120 mg/ml of K_2HPO_4 whereas BMD based on patient's CT scans was established to be 165 mg/ml of K_2HPO_4. It is possible that calibration of measured HU to BMD differs for diverse CT scanners and so phantom-less calibration was performed. Nevertheless, phantom-less calibration led to even higher values of BMD and so the previous regression model was used eventually [50].

Reviewing the previous experiments, it was also revealed that BMD measured in mg of K_2HPO_4 was sometimes mistaken for one using CaHA calibration rods, even though these values represent two different bone densities. Lu et al., 2014, defined a relation between these mineral densities implying that BMD measured in mg of K_2HPO_4 is lower than the one measured in CaHA [63]. Although carefully following the process of establishment, the source of difference between mean BMD according to Brinckmann et al., 1988, and the one measured in this study was not found and thus both of the values were used for calculations. Reviewing the other studies, BMD varied between 180-230 mg/ml in K_2HPO_4 which is in accordance with the measurement performed in this study [49, 50].

The results of this study are subjected to many input parameters which can significantly influence the findings. Beside that, the studied case of an epileptic patient is a complex problem which cannot be solved precisely and a lot of assumptions and simplifiations had to be accepted. The aim of this study, however, was not to provide an exact solution but to provide a basic engineering insight into the fracture meachanism during an epileptic seizure. The results showed that compressive vertebral fracture can indeed be caused by an extreme muscle stretch.

Chapter 7

Conclusion

Vertebral fractures after an epileptic seizure with no external trauma may occur during an epileptic seizure even though the patient is in a sitting or laying position and does not undergo any external trauma. The studies highlighted that the symptoms might be mild and resemble simple acute mechanical back pain which is often treated with spinal mobilization and adjustments. This treatement in case of a vertebral fracture may considerably threaten the patient as it presents a complete contradiction: It may increase pain and prolong disability or cause spinal cord injuries. To eliminate the misdiagnosis of such cases, the awareness of the potential risk of vertebral fracture caused by an extreme muscle stretch should be increased among the doctors.

This study aimed to support the initial hypothesis that an extreme stretch of back muscles might result in vertebral compressive fracture. Providing the patient-specific biomechanical analysis, the risk of vertebral fracture during the seizure was estimated. To evaluate the risk of fracture, predicted vertebral ultimate load was compared to estimated muscle forces compressing individual veretbrae of patient's thoracic spine. To be able to estimated the compressive force acting on each vertebra, firstly, the computational model had to be defined and the assessment of parameters required for analysis and elimination of muscle fascicles involved in the analysis followed. Eventually, the forces were calculated from equilibrium at each vertebral level. To estimate the compressive failure load, regression model was used. Parameters of the given vertebra correlated to its failure load included CSA and BMD which were both measured from patient's CT scans.

It was found that estimated muscle forces, under some extreme circumstances, can exceed the vertebral compressive failure load and thus result in vertebral fracture. Providing the computational support, it is believed that the awareness of this phenomenom will spread and the number of misdiagnosed seizure-induced vertebral fractures will be eliminated. The study indicates a need for modification of the standard clinical practice guidelines for epilepsy. CT examination should be performed if the patient complains of any back pain after an epileptic seizure even though the sizure is unrelated to any external trauma.

Appendices

Appendix A

Global coordinates of the joints

Table A.1: Vertical position of the vertebral joints, assigned to the vertebra located below the joint.

Vertebra	**Position [m]**
T1	0.565
T2	0.546
T3	0.526
T4	0.504
T5	0.480
T6	0.454
T7	0.430
T8	0.405
T9	0.382
T10	0.358
T11	0.331
T12	0.304
L1	0.274
L2	0.243
L3	0.212
L4	0.177
L5	0.140

Appendix B

Muscle groups

Table B.1: List of the muscles groups included in the analysis after muscle elimination. Each muscle is divided into individual fascicles represented by its isometric force. Values taken over from the musculoskeletal model made by Bruno et al. [37].

Muscle Name	**PCSA [cm2]**	α [°]	**Fiso [N]**
Latissimus Dorsi			
LD_L1_r	0.90	0.0	90.40
LD_L2_r	0.85	0.0	84.54
LD_L3_r	1.05	0.0	104.52
LD_L4_r	1.01	0.0	100.73
LD_L5_r	1.02	0.0	101.69
LD_T12_r	0.54	0.0	53.71
LD_T11_r	0.63	0.0	62.92
LD_T10_r	0.64	0.0	64.48
LD_T9_r	0.41	0.0	40.62
LD_T8_r	0.41	0.0	40.79
LD_T7_r	0.37	0.0	37.07
LD_R12_r	0.43	0.0	42.90
LD_R11_r	0.63	0.0	63.33
LD_Il_r	0.65	0.0	65.37
Erector Spinae			
IL_L1_r	1.47	13.8	147.44
IL_L2_r	1.83	13.8	183.22
IL_L3_r	2.17	13.8	216.76
IL_L4_r	4.15	13.8	414.91

Muscle Name	PCSA [cm2]	α [°]	Fiso [N]
L_R5_r	0.57	13.8	57.32
IL_R6_r	0.73	13.8	72.69
IL_R7_r	0.88	13.8	87.66
IL_R8_r	0.78	13.8	77.92
IL_R9_r	0.96	13.8	95.91
IL_R10_r	1.92	13.8	191.84
IL_R11_r	2.35	13.8	235.18
IL_R12_r	2.06	13.8	206.17
LTpT_T1_r	3.26	12.6	325.89
LTpT_T2_r	2.41	12.6	240.66
LTpT_T3_r	1.73	12.6	172.50
LTpT_T4_r	0.61	12.6	60.58
LTpT_T5_r	0.57	12.6	57.01
LTpT_T6_r	0.81	12.6	81.41
LTpT_T7_r	0.80	12.6	79.71
LTpT_T8_r	1.20	12.6	120.47
LTpT_T9_r	1.39	12.6	139.43
LTpT_T10_r	1.21	12.6	120.51
LTpT_T11_r	1.15	12.6	115.08
LTpT_T12_r	0.94	12.6	94.29
LTpT_R4_r	0.60	12.6	60.50
LTpT_R5_r	0.57	12.6	56.96
LTpT_R6_r	0.81	12.6	81.41
LTpT_R7_r	0.80	12.6	79.71
LTpT_R8_r	1.30	12.6	130.02
LTpT_R9_r	1.11	12.6	110.68
LTpT_R10_r	1.20	12.6	120.42
LTpT_R11_r	1.15	12.6	115.39
LTpT_R12_r	0.94	12.6	94.33
LTpL_L5_r	1.58	12.6	157.80
LTpL_L4_r	1.52	12.6	151.84
LTpL_L3_r	1.21	12.6	121.28
LTpL_L2_r	1.08	12.6	108.38
LTpL_L1_r	1.06	12.6	106.16
Multifidus			
MF_m1s_r	0.81	0.0	81.20
MF_m1t_1_r	0.72	0.0	71.96
MF_m1t_2_r	0.60	0.0	59.73
MF_m1t_3_r	1.00	0.0	99.76
MF_m2s_r	0.54	0.0	54.48
MF_m2t_1_r	0.57	0.0	57.47
MF_m2t_2_r	1.46	0.0	145.89

Muscle Name	PCSA [cm2]	α [°]	Fiso [N]
MF_m2t_3_r	1.61	0.0	161.19
MF_m3s_r	0.84	0.0	83.72
MF_m3t_1_r	0.91	0.0	90.98
MF_m3t_2_r	0.91	0.0	90.98
MF_m3t_3_r	0.91	0.0	90.98
MF_m4s_r	1.01	0.0	101.07
MF_m4t_1_r	0.90	0.0	90.12
MF_m4t_2_r	0.90	0.0	90.12
MF_m4t_3_r	0.90	0.0	90.12
MF_m5s_r	0.35	0.0	34.88
MF_m5t_1_r	0.35	0.0	34.88
MF_m5t_2_r	0.35	0.0	34.88
MF_m5t_3_r	0.35	0.0	34.88
MF_m1_laminar_r	0.39	0.0	39.05
MF_m2_laminar_r	0.31	0.0	30.97
MF_m3_laminar_	0.36	0.0	35.78
MF_m4_laminar_r	0.26	0.0	25.95
MF_m5_laminar_r	0.56	0.0	55.94
supmult-T1-C4	2.84	5.0	283.66
supmult-T1-C5	2.84	5.0	283.66
supmult-T2-C6	2.84	5.0	283.66
deepmult-T1-C5	2.84	5.0	283.66
deepmult-T1-C6	2.84	5.0	283.66
deepmult-T2-C7	2.84	5.0	283.66
deepmult-T2-T1	2.84	5.0	283.66
multifidus_L2_T12	2.29	5.0	229.35
multifidus_L1_T11	2.41	5.0	241.13
multifidus_T12_T10	2.25	5.0	224.73
multifidus_T11_T9	2.20	5.0	219.50
multifidus_T10_T8	1.85	5.0	184.60
multifidus_T9_T7	1.54	5.0	154.00
multifidus_T8_T6	1.99	5.0	198.96
multifidus_T7_T5	2.52	5.0	251.55
multifidus_T6_T4	2.84	5.0	283.66
multifidus_T5_T3	2.84	5.0	283.66
multifidus_T4_T2	2.84	5.0	283.66
multifidus_T3_T1	2.84	5.0	283.66

Muscle Name	PCSA [cm2]	α [°]	Fiso [N]
Quadratus Lumborum			
QL_post_I_1-L3_r	0.76	7.4	75.59
QL_post_I_2-L4_r	1.56	7.4	156.41
QL_post_I_2-L3_r	0.59	7.4	58.56
QL_post_I_2-L2_r	0.37	7.4	36.55
QL_post_I_3-L1_r	0.77	7.4	77.19
QL_post_I_3-L2_r	0.56	7.4	56.49
QL_post_I_3-L3_r	0.96	7.4	96.36
QL_mid_L3-12_3_r	0.42	7.4	41.93
QL_mid_L3-12_2_r	0.48	7.4	47.72
QL_mid_L3-12_1_r	0.80	7.4	79.53
QL_mid_L2-12_1_r	1.56	7.4	156.09
QL_mid_L4-12_3_r	0.42	7.4	42.10
QL_ant_I_2-T12_r	0.45	7.4	45.39
QL_ant_I_3-T12_r	0.85	7.4	85.28
QL_ant_I_2-12_1_r	0.28	7.4	28.08
QL_ant_I_3-12_1_r	0.53	7.4	53.17
QL_ant_I_3-12_2_r	0.35	7.4	35.25
QL_ant_I_3-12_3_r	0.41	7.4	40.63
Trapezius			
trap_inf_T4	0.68	0.0	67.65
trap_inf_T5	0.68	0.0	67.65
trap_inf_T6	0.79	0.0	78.86
trap_inf_T7	0.77	0.0	77.17
trap_inf_T8	0.72	0.0	72.05
trap_inf_T9	0.66	0.0	66.05
trap_inf_T10	0.62	0.0	61.51
trap_inf_T11	0.59	0.0	59.02
trap_inf_T12	0.59	0.0	58.90
Neck Muscles			
splen_cap_skl_T	0.71	0.0	70.73
splen_cap_skl_T2	0.71	0.0	70.73
splen_cerv_c3_T3	0.35	0.0	35.36
splen_cerv_c3_T4	0.35	0.0	35.36
splen_cerv_c3_T5	0.35	0.0	35.36
splen_cerv_c3_T6	0.35	0.0	35.36
longissi_cerv_c4thx	0.57	0.0	57.29
long_col_c1thx	0.27	5.0	27.34
long_col_c5thx	0.27	5.0	27.34
iliocost_cerv_c5rib	0.57	0.0	57.29

Appendix C

Angles of vertebral mid-planes

Table C.1: Angles between the tranverse plane and the vertebral mid-plane measured from patient's CT scans.

	Angle [°]				
Vertebra	**Mean**	**Std**	**Vertebra**	**Mean**	**Std**
T1	-28.39	2.04	T7	1.34	0.56
T2	-25.66	1.17	T8	3.18	0.76
T3	-25.59	1.81	T9	6.50	0.80
T4	-15.58	2.03	T10	12.53	1.30
T5	-12.26	0.89	T11	13.35	1.03
T6	-1.30	0.53	T12	15.51	0.81

Appendix D

Muscles included in the analysis

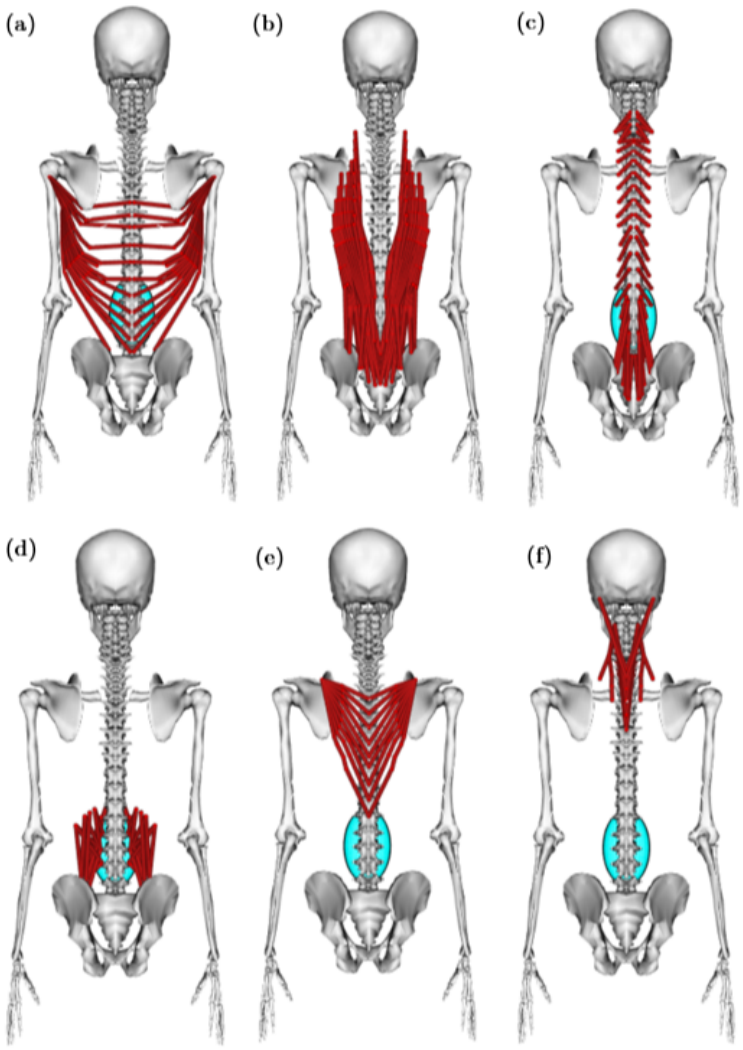

Figure D.1: Depiction of the back muscles included in the analysis. (a) Latissimus dorsi, (b) erector spinae, (c) multifidus, (d) quadratus lumborum (e) trapezius (f) neck muscles .

References

[1] Fisher, Robert S., Walter van Emde Boas, Warren Blume, Christian Elger, Pierre Genton, Phillip Lee, and Jerome Engel. "Epileptic Seizures and Epilepsy: Definitions Proposed by the International League Against Epilepsy (ILAE) and the International Bureau for Epilepsy (IBE)." *Epilepsia* 46, no. 4 (April 2005): 470-72.

[2] Coben, Robert, and Iman Mohammad-Rezazadeh. "Neural Connectivity in Epilepsy as Measured by Granger Causality." *Frontiers in Human Neuroscience 9* (July 2015).

[3] Chang, Bernard S., and Daniel H. Lowenstein. "Epilepsy." *New England Journal of Medicine* 349, no. 13 (October 2003).

[4] Kiriakopoulos, Elaine, and Patricia O. Shafer. "Types of Seizures." Epilepsy Foundation. https://www.epilepsy.com/learn/types-seizures (accessed May 15, 2018).

[5] Lava, Neil. "Types of Seizures and Their Symptoms." WebMD Medical Reference. https://www.webmd.com/epilepsy/types-of-seizures-their-symptoms (accessed May 15, 2018).

[6] Napier, R. J., and P. C. Nolan. "Diagnosis of vertebral fractures in post-ictal patients." *Emergency Medicine Journal* 28, no. 2 (November 2011): 169-70.

[7] McKean, Sylvia C. *Principles and Practice of Hospital Medicine.* New York: McGraw-Hill, 2012.

[8] Kelly, J. P. "Fracture complicating electro-convulsive therapy and chronic epilepsy." *J Bone Joint Surg 36* (1954): 70–9.

[9] Mattson, Richard H., and Barry E. Gidal. "Fractures, epilepsy, and antiepileptic drugs." *Epilepsy & Behavior 5* (February 2003): 36-40.

[10] Vasconcelos, Daniel. "Compression Fractures of the Vertebrae during Major Epileptic Seizures." *Epilepsia 14*, no. 3 (October 1973): 323-28.

[11] Takahashi, Toshiyuki, Teiji Tominaga, Hiroshi Shamoto, Hiroaki Shimizu, and Takashi Yoshimoto. "Seizure-induced thoracic spine compression fracture." *Surgical Neurology 58*, no. 3-4 (October 2002): 214-16.

[12] Gnanalingham, K., M. Macanovic, S. Joshi, F. Afshar, and J. Yeh. "Non-Traumatic Compression Fractures of the Thoracic Spine Following a Seizure - Treatment by Percutaneous Kyphoplasty." *Minimally Invasive Neurosurgery 47*, no. 4 (September 2004): 256-57.

[13] Mehlhorn, AT, P.C. Strohm, O. Hausschildt, H. Schmal, N.P Südkamp. "Seizure-induced muscle force can caused lumbar spine fracture." *Acta Chir Orthop Traumatol Cech 73*, no. 3 (June 2007): 202-5

[14] Moscote-Salazar, Luis Rafael, Andres M. Rubiano, Hernando Raphael Alvis-Miranda, and Gabriel Alcala-Cerra. "Non traumatic fractures of the lumbar spine and seizures: case report." *Romanian Neurosurgery 29*, no. 4 (January 2015).

[15] Stilwell, Peter, Katherine Harman, William Hsu, and Brian Seaman. "Multiple seizure-induced thoracic vertebral compression fractures: a case report." *J Can Chiropr Assoc. 60*, no. 3 (September 2016): 252–257.

[16] Youssef, J.A. , G.M. McCullen, C.C. Brown. "Seizure-induced lumbar burst fracture." *Spine 20* (1995), no. 11: 1301–3.

[17] Ballock, R.T., R. Mackersie, J.J. Abitbol, V. Cervilla, D. Resnick, S.R Garfin. "Can burst fractures be predicted from plain radiographs?" *J Bone Joint Surg Br. 74*, no. 1 (January 1992): 147-50.

[18] Brakeville, Ross. "Treatment for Spinal Compression Fractures." WebMD. https://www.webmd.com/pain-management/guide/spinal-compression-fractures-treatments (accessed May 30, 2018).

[19] Phillips, Frank M. "Minimally Invasive Treatments of Osteoporotic Vertebral Compression Fractures." *Spine 28*, no. supplement (September 1976): S45-S53.

[20] McCall, Todd, Chad Cole, and Andrew Dailey. "Vertebroplasty and kyphoplasty: a comparative review of efficacy and adverse events." Current Reviews in Musculoskeletal Medicine 1, no. 1 (January 2008): 17-23.

[21] Ringer, Andrew. "Vertebroplasty and Kyphoplasty." Mayfield Brain & Spine. https://www.mayfieldclinic.com/PDF/PE-Kyphoplasty.pdf (accessed May 30, 2018).

[22] Bohinski, Robert. "Anterior Cervical Discectomy & Fusion." Mayfield Brain & Spine. https://www.mayfieldclinic.com/PDF/PE-ACDF.pdf (accessed May 30, 2018).

[23] Highsmith, Jason M. "What Is Spinal Instrumentation and Spinal Fusion?" SpineUniverse. https://www.spineuniverse.com/treatments/surgery/what-spinal-instrumentation-spinal-fusion (accessed May 30, 2018).

[24] Hall, Susan J. *Basic Biomechanics.* New York, NY: McGraw-Hill Education, 2015.

[25] Buchaman, Thomas S., David G. Lloyd, Kurt Manal, and Thor F. Besier. "Estimation of Muscle Forces and Joint Moments Using a Forward-Inverse Dynamics Model." *Medicine & Science in Sports & Exercise 37*, no. 11 (December 2005): 1911-16.

[26] McGill, Stuart M., Leigh Marshall, and Jordan Andersen. "Low back loads while walking and carrying: comparing the load carried in one hand or in both hands." *Ergonomics 56*, no. 2 (February 2012): 293-302.

[27] Dreischarf, Marcel, Antonius Rohlmann, Rui Zhu, Hendrik Schmidt, and Thomas Zander. "Is it possible to estimate the compressive force in the lumbar spine from intradiscal pressure measurements? A finite element evaluation." *Medical Engineering & Physics 35*, no. 9 (October 2013): 1385-90.

[28] Rohlmann, Antonius, David Pohl, Alwina Bender, Friedmar Graichen, Jörn Dymke, Hendrik Schmidt, and Georg Bergmann. "Activities of Everyday Life with High Spinal Loads." *PLoS ONE 9*, no. 5 (May 2014): e98510.

[29] Wilke, Hans–Joachim, Peter Neef, Marco Caimi, Thomas Hoogland, and Lutz E. Claes. "New In Vivo Measurements of Pressures in the Intervertebral Disc in Daily Life." *Spine 24*, no. 8 (April 1999): 755-62.

[30] Dreischarf, Marcel, Antonius Rohlmann, Rui Zhu, Hendrik Schmidt, and Thomas Zander. "Is it possible to estimate the compressive force in the lumbar spine from intradiscal pressure measurements? A finite element evaluation." *Medical Engineering & Physics 35*, no. 9 (October 2013): 1385-90.

[31] Michael A. Adams, *The Biomechanics of Back Pain*, 3rd ed. (Edinburgh: Churchill Livingstone/Elsevier, ©2013), 115-19.

[32] Hong, Youlian, and Roger Bartlett, eds. *Routledge Handbook of Biomechanics and Human Movement Science.* Routledge International Handbooks. London: Routledge, 2008.

[33] Levangie, Pamela K., and Cynthia C. Norkin. *Joint Structure and Function: A Comprehensive Analysis.* 4th ed. Philadelphia, PA: F.A. Davis Co., ©2005.

[34] Delp, Scott L., Frank C. Anderson, Allison S. Arnold, Peter Loan, Ayman Habib, Chand T. John, Eran Guendelman, and Darryl G. Thelen. "OpenSim: Open-Source Software to Create and Analyze Dynamic Simulations of Movement." *IEEE Transactions on Biomedical Engineering 54*, no. 11 (December 2007): 1940-50.

[35] Craig, R. *The structure of the contract filaments.* Myology, New York: McGraw-Hill Education, 1994.

[36] Arnold, Edith M., Samuel R. Ward, Richard L. Lieber, and Scott L. Delp. "A Model of the Lower Limb for Analysis of Human Movement." *Annals of Biomedical Engineering 38*, no. 2 (February 2010): 269-79.

[37] Bruno, Alexander G., Mary L. Bouxsein, and Dennis E. Anderson. "Development and Validation of a Musculoskeletal Model of the Fully Articulated Thoracolumbar Spine and Rib Cage." *Journal of Biomechanical Engineering* 137, no. 8 (June 2015): 081003.

[38] Vasavada, Anita N., Songsong Li and Scott L. Delp. "Influence of muscle morphometry and moment arms on the moment-generating capacity of human neck muscles." *Spine 23*, no. 4 (1998): 412-22.

[39] Holzbaur, Katherine R. S., Wendy M. Murray, and Scott L. Delp. "A Model of the Upper Extremity for Simulating Musculoskeletal Surgery and Analyzing Neuromuscular Control." *Annals of Biomedical Engineering 33*, no. 6 (June 2005): 829-40.

[40] Leva, Paolo de. "Adjustments to Zatsiorsky-Seluyanov's segment inertia parameters." *Journal of biomechanics 29*, no9 (1996): 1223-30.

[41] Pearsall, David J., J. Gavin Reid, and Lori A. Livingston. "Segmental inertial parameters of the human trunk as determined from computed tomography." *Annals of Biomedical Engineering 24*, no. 2 (March 1996): 198-210.

[42] M. Christophy. "A detailed open-source musculoskeletal model of the human lumbar spine." Master's thesis, University of California at Berkeley, 2010.

[43] Morita, Daigo, Yasutsugu Yukawa, Hiroaki Nakashima, Keigo Ito, Go Yoshida, Masaaki Machino, Syunsuke Kanbara, Toshiki Iwase, and Fumihiko Kato. "Range of motion of thoracic spine in sagittal plane." *European Spine Journal* 23, no. 3 (December 2014): 673-78.

[44] Narici, Marco. "Human skeletal muscle architecture studied in vivo by non-invasive imaging techniques: functional significance and applications." *Journal of Electromyography and Kinesiology* 9, no. 2 (April 1999): 97-103.

[45] Mayers, Elizabeth R. and Sara E. Wilson. "Biomechanics of osteoporosis and vertebral fracture." *Spine*, no. 22 (1997): 25S-31S.

[46] Bachmann, Katherine N, Alexander G Bruno, Miriam A Bredella, Melanie Schorr, Elizabeth A Lawson, Corey M Gill, Vibha Singhal, Erinne Meenaghan, Anu V Gerweck, Kamryn T Eddy, Seda Ebrahimi, Stuart L Koman, James M Greenblatt, Robert J Keane, Thomas Weigel, Esther Dechant, Madhusmita Misra, and Anne Klibanski. "Vertebral Strength and Estimated Fracture Risk Across the BMI Spectrum in Women." *Journal of Bone and Mineral Research 31*, no. 2 (October 2017): 281-88.

[47] Bouxsein, Mary L, L Joseph Melton, B Lawrence Riggs, John Muller, Elizabeth J Atkinson, Ann L Oberg, Richard A Robb, Jon J Camp, Peggy A Rouleau, Cynthia H McCollough, and Sundeep Khosla. "Age- and Sex-Specific Differences in the Factor of Risk for Vertebral Fracture: A Population-Based Study Using QCT." *Journal of Bone and Mineral Research 21*, no. 9 (June 2006): 1475-82.

[48] Brinckmann, P., M. Biggemann, and D. Hilweg. "Prediction of the compressive strength of human lumbar vertebrae." *Clinical Biomechanics* 4 (January 1988): iii-27.

[49] Bruno, Alexander G, Kerry E Broe, Xiaochun Zhang, Elizabeth J Samelson, Ching-An Meng, Rajaram Manoharan, John D'Agostino, L Adrienne Cupples, Douglas P Kiel, and Mary L Bouxsein. "Vertebral Size, Bone Density, and Strength in Men and Women Matched for Age and Areal Spine BMD." *Journal of Bone and Mineral Research 29*, no. 3 (February 2014): 562-69.

[50] Singer, K., S. Edmondston, R. Day, P. Breidahl, and R. Price. "Prediction of thoracic and lumbar vertebral body compressive strength: correlations with bone mineral density and vertebral region." *Bone 17*, no. 2 (September 1995): 167-74.

[51] Crawford, R.Paul, Christopher E. Cann, and Tony M. Keaveny. "Finite element models predict in vitro vertebral body compressive strength better than quantitative computed tomography." *Bone 33*, no. 4 (November 2003): 744-50.

[52] Kopperdahl, David L., Elise F. Morgan, and Tony M. Keaveny. "Quantitative computed tomography estimates of the mechanical properties of human vertebral trabecular bone." *Journal of Orthopaedic Research 20*, no. 4 (July 2001): 801-5.

[53] Hansson, T., B. Roos, A. Nachemson. "The bone mineral content and ultimate compressive strength of lumbar vertebrae." *Spine 5*, no. 1 (January 1980): 46-55.

[54] Kopperdahl, David L, and Tony M Keaveny. "Yield strain behavior of trabecular bone." *Journal of Biomechanics 31*, no. 7 (July 1998): 601-8.

[55] Celenk, Cetin, and Peruze Celenk. "Bone Density Measurement Using Computed Tomography." *Computed Tomography - Clinical Applications* (January 2012), 123-236.

[56] Weaver, Ashley A., Kristen M. Beavers, R. Caresse Hightower, Sarah K. Lynch, Anna N. Miller, and Joel D. Stitzel. "Lumbar Bone Mineral Density Phantomless Computed Tomography Measurements and Correlation with Age and Fracture Incidence." *Traffic Injury Prevention 16*, no. sup2 (November 2015): S153-S160.

[57] Cann, C.E., and Genant H.K.. "Precise measurement of vertebral mineral content using computed tomography." *J Comp Assist Tomog 4* (1980): 493-500.

[58] Bernaciková, Martina, Miriam Kalichová,Lenka Beránková. "Segmenty těla, těžiště těla." Základy sportovní kineziologie. https://is.muni.cz/do/1451/e-learning/kineziologie/elportal/pages/segmentyteziste.html (accessed May 15, 2018).

[59] van Arkel, Richard J., Luca Modenese, Andrew T.M. Phillips, and Jonathan R.T. Jeffers. "Hip abduction can prevent posterior edge loading of hip replacements." *Journal of Orthopaedic Research* 31, no. 8 (April 2013): 1172-79.

[60] Phillips, Andrew T.M., Claire C. Villette, and Luca Modenese. "Femoral bone mesoscale structural architecture prediction using musculoskeletal and finite element modelling." *International Biomechanics* 2, no. 1 (January 2015): 43-61.

[61] Schindelin, Johannes, Ignacio Arganda-Carreras, Erwin Frise, Verena Kaynig, Mark Longair, Tobias Pietzsch, Stephan Preibisch, Curtis Rueden, Stephan Saalfeld, Benjamin Schmid, Jean-Yves Tinevez, Daniel James White, Volker Hartenstein, Kevin Eliceiri, Pavel Tomancak, and Albert Cardona. "Fiji: an open-source platform for biological-image analysis." *Nature Methods* 9, no. 7 (July 2012): 676-82.

[62] Schneider, C. A., W. S. Rasband, K. W. Eliceiri. "NIH Image to ImageJ: 25 years of image analysis", *Nature methods* 9, no. 7 (2012): 671-675.

[63] Lu, Yongtao, Klaus Engelke, Claus-C Glueer, Michael M Morlock, and Gerd Huber. "The effect of in situ/in vitro three-dimensional quantitative computed tomography image voxel size on the finite element model of human vertebral cancellous bone." *Proceedings of the Institution of Mechanical Engineers, Part H: Journal of Engineering in Medicine* 228, no. 11 (December 2014): 1208-13.